

See discussions, stats, and author profiles for this publication at: <https://www.researchgate.net/publication/267751860>

# Molecular Modeling and Gas Permeation Properties of a Polymer of Intrinsic Microporosity Composed of Ethanoanthracene and Tröger's Base Units

ARTICLE *in* MACROMOLECULES · NOVEMBER 2014

Impact Factor: 5.8 · DOI: 10.1021/ma501469m

---

CITATIONS

3

READS

121

## 16 AUTHORS, INCLUDING:



Elena Tocci

Italian National Research Council

40 PUBLICATIONS 478 CITATIONS

[SEE PROFILE](#)



Neil B. McKeown

The University of Edinburgh

209 PUBLICATIONS 7,270 CITATIONS

[SEE PROFILE](#)



Mariolino Carta

The University of Edinburgh

49 PUBLICATIONS 578 CITATIONS

[SEE PROFILE](#)



Johannes Carolus (John) Jansen

Italian National Research Council

105 PUBLICATIONS 1,828 CITATIONS

[SEE PROFILE](#)

## Molecular Modeling and Gas Permeation Properties of a Polymer of Intrinsic Microporosity Composed of Ethanoanthracene and Tröger's Base Units

Elena Tocci,<sup>\*,†</sup> Luana De Lorenzo,<sup>†</sup> Paola Bernardo,<sup>†</sup> Gabriele Clarizia,<sup>†</sup> Fabio Bazzarelli,<sup>†</sup> Neil B. McKeown,<sup>‡</sup> Mariolino Carta,<sup>‡</sup> Richard Malpass-Evans,<sup>‡</sup> Karel Friess,<sup>§</sup> Kryštof Pilnáček,<sup>§</sup> Marek Lanč,<sup>§</sup> Yuri P. Yampolskii,<sup>||</sup> Ludmila Strarannikova,<sup>||</sup> Viktor Shantarovich,<sup>⊥</sup> Michele Mauri,<sup>#</sup> and Johannes C. Jansen<sup>\*,†</sup>

<sup>†</sup>Institute on Membrane Technology, ITM-CNR, Via P. Bucci, Cubo 17/C, 87036 Rende (CS), Italy

<sup>‡</sup>School of Chemistry, University of Edinburgh, Joseph Black Building, West Mains Road, Edinburgh EH9 3JJ, U.K.

<sup>§</sup>Department of Physical Chemistry, Institute of Chemical Technology, Technická 5, Prague 6, 166 28, Czech Republic

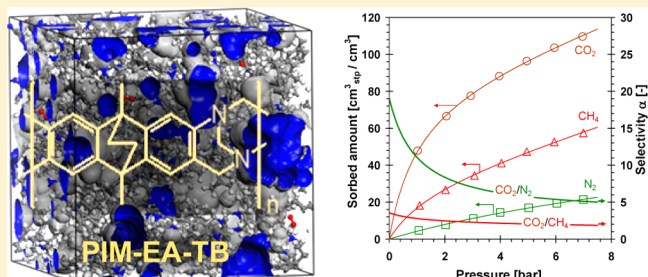
<sup>||</sup>A.V. Topchiev Institute of Petrochemical Synthesis, Russian Academy of Sciences, 29 Leninsky Prospect, 119991, Moscow, Russia

<sup>⊥</sup>N. N. Semenov Institute of Chemical Physics, Russian Academy of Sciences, 4 Kosygin Street, 117334, Moscow, Russia

<sup>#</sup>Department of Materials Science, University of Milano-Bicocca, Via R. Cozzi 55, 20125, Milan, Italy

### Supporting Information

**ABSTRACT:** Polymers of intrinsic microporosity (PIMs) are receiving increasing attention from the membrane community because of their high gas and vapor permeability. Recently a novel ethanoanthracene-based PIM synthesized by Tröger's base formation (PIM-EA-TB) was reported to have exceptional transport properties, behaving as a polymer molecular sieve membrane. In the present work, an extensive investigation of the structural, mechanical, and transport properties of this polymer, both by experimental analysis and by molecular simulation, offers deep insight into the behavior of this polymer and gives an explanation for its remarkable performance as a membrane material. Transport properties were determined by the barometric time-lag method, by the volumetric method with gas chromatographic or mass spectrometric gas analysis, and by gravimetric sorption measurements, yielding all basic transport parameters, permeability ( $P$ ), diffusivity ( $D$ ), and solubility ( $S$ ). Upon alcohol treatment, PIM-EA-TB exhibited a much stronger permeability increase than archetypal "benchmark" polymer PIM-1, with performance above the Robeson upper bound for several gas pairs. This is in part due to an extremely high gas solubility in PIM-EA-TB, higher than in PIM-1. The experimental data were supported by extensive modeling studies of the polymer structure and the spatial arrangement of its free volume. Modeling confirms that the high gas permeability must be attributed to the large fractional free volume of the polymer. The simulated free volume size distribution in PIM-EA-TB is in agreement with the average experimental free volume elements size determined by PALS and  $^{129}\text{Xe}$  NMR analysis. The modeled spatial arrangement of the free volume revealed a slightly lower interconnectivity of the FV elements in PIM-EA-TB compared to PIM-1. Along with its higher chain rigidity, determined by analysis of the torsion angles in the polymer model, this was identified as the main reason for its stronger size sieving behavior and relatively high permselectivity. A number of peculiarities in the behavior of PIMs will also be discussed here, explaining discrepancies between results published in the literature by different laboratories, the effect of their thermomechanical history, aging, or conditioning, and the influence of the measurement technique and of the experimental conditions on the results. This makes this study of inestimable value for unifying the results of different experimental techniques and fully understanding the transport properties.



## 1. INTRODUCTION

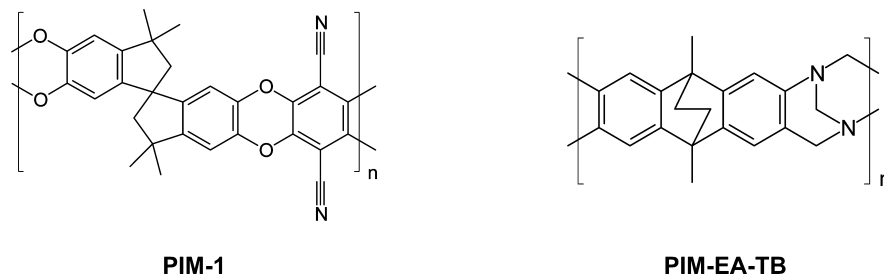
The development of polymers of intrinsic microporosity (PIMs) was an important event of the past decade in membrane science.<sup>1,2</sup> In particular, the first representative of this group, PIM-1,<sup>3</sup> whose structure is shown in Scheme 1, has been the subject of detailed studies by several groups of membrane researchers since it was first reported almost a decade ago.<sup>4–8</sup>

PIMs are distinguished by several unusual and interesting properties making them attractive membrane materials: (1) possibility to strongly control their gas permeation parameters by

Received: July 17, 2014

Revised: October 17, 2014



**Scheme 1.** Molecular Structure of the Archetypal PIM-1 and the More Recent PIM-EA-TB

a well-defined protocol of film treatment; (2) good combination of the permeability coefficients and separation factors: the data points of PIM-1 define the 2008 upper bound on Robeson diagrams (selectivity vs permeability) for some important gas pairs;<sup>9</sup> (3) extremely large solubility coefficients, which are the largest among all polymer classes studied for gas separation membranes; (4) ready processability from solution; (5) high free volume. All this makes PIM-1 and its structural analogues very promising next generation membrane materials. However, many aspects of their exceptional behavior remain still unknown, necessitating careful further studies.

Recently, the exceptional properties of the novel PIM-EA-TB (Scheme 1), were described.<sup>10</sup> The high backbone rigidity induced by the Tröger's base moiety<sup>11</sup> gives this polymer an enhanced size-sieving behavior as compared to other PIMs, providing greater selectivity for various gas pairs. However, its performance for the important CO<sub>2</sub>/N<sub>2</sub> and CO<sub>2</sub>/CH<sub>4</sub> gas pairs appears unremarkable relative to other PIMs, suggesting to perform a deeper study of this material, comparing its properties with those of the archetypal PIM-1 to gain more fundamental understanding of its properties.

A traditional and seemingly well-established paradigm of membrane science is that the gas permeation parameters of a polymer and the position of the corresponding data points on Robeson's diagrams are determined primarily by the chemical structure of the polymers.<sup>12,13</sup> However, during the past decade it has become apparent that other factors can affect the observed permeability coefficients of polymers. For example, it was demonstrated that, depending on the protocol of poly(ether imide) film preparation and particularly the presence of residual solvent (CHCl<sub>3</sub>), entirely different permeability coefficients can be attained,<sup>14</sup> with some data points above the upper bound of 1991,<sup>13</sup> with an increase of both the separation factor  $\alpha(O_2/N_2)$  and the permeability coefficient  $P(O_2)$  by a factor 4. Such behavior is even more typical for high free volume, highly permeable polymers. Thus, for poly(trimethylsilyl propyne) (PTMSP) quite different values of  $P(O_2)$  have been reported: from 3000<sup>15</sup> to 9000 Barrer.<sup>16</sup> In many cases the effects of film pretreatment and physical aging are responsible for these phenomena.<sup>17,18</sup> Preconditioning of the PTMSP films with methanol (nonsolvent and a swelling agent for this polymer) is often used to erase a prior history of a sample.<sup>18</sup> Alcohol-conditioned PTMSP films have a significantly higher free volume and permeability than unconditioned films. Similar effects have been observed for PIM-1. It was shown that the permeability coefficients of this polymer differed by 1 order of magnitude, depending on the film preparation protocol:  $P(O_2)$  was reported to be 150 Barrer for the film contacted with water before permeability measurement, while 1600 Barrer was measured for the film immersed into lower alcohols.<sup>5</sup> An explanation of these phenomena can be given based on swelling (as in the case of PTMSP) or formation of hydrogen

bonds between acid hydrogen atoms of alcohols and water and oxygen atoms of the dioxane ring of PIM-1.<sup>19</sup> Something similar is observed for PIM-EA-TB as will be seen from subsequent sections of the present work.

In this work, the fundamental aspects of the transport properties in PIM-EA-TB will be further investigated by comparing the results of different experimental techniques and computer modeling. The gas transport parameters, free volume and thermodynamic properties of PIM-EA-TB are investigated in comparison with those in PIM-1. Using several experimental techniques, it will be demonstrated how sample conditioning substantially influences the transport parameters. This is one of the reasons why for highly permeable membrane materials, in particular those based on PIMs, a considerable scatter in the data is often observed in the literature. Modeling studies will provide a computational basis for the experimentally determined solubility and diffusion coefficients of several gases. Besides the aspect of the validation of the obtained packing models through the transport properties, further analysis of the models yields information about the flexibility of the polymer matrix and the free volume distribution in PIM-EA-TB and elucidates the role of the molecular and structural properties in the exceptional permeation properties of this polymer, such as the high O<sub>2</sub>/N<sub>2</sub> ideal selectivity. Experimental support for the free volume distribution is obtained from Positron Annihilation Lifetime Spectroscopy (PALS) and <sup>129</sup>Xe NMR spectroscopy. PALS is the most acknowledged method for determination of free volume in polymers. On the other hand, <sup>129</sup>Xe chemical shift is sensitive to the shape, size and nature of the local environment. Having a van der Waals diameter of 0.44 nm and high affinity for apolar and aromatic systems, the xenon atom can explore a wide range of nanosized structures including polymers,<sup>20</sup> porous crystals,<sup>21</sup> clays,<sup>22</sup> and natural materials.<sup>23</sup> Modeling studies allow the use of basically any kind of probe, from a dimensionless particle to positrons or even the same gas molecules used for experimental permeability tests. Molecular simulation is also the only available approach that can provide direct information on the spatial arrangement of the free volume, rather than just the size and shape. This is of inestimable value for unifying the result of different experimental techniques and fully understanding the transport properties. Therefore, a substantial part of the present paper will be dedicated to modeling studies.

## 2. EXPERIMENTAL SECTION

**2.1. Membrane Preparation.** Thin film flat membranes were prepared by solvent evaporation from a 2–4% w/v solution of PIM-EA-TB in chloroform (typically 600 mg in 18 mL of chloroform) as described previously.<sup>10</sup> The solution was filtered through glass wool to remove dust and poured into a 9 cm circular Teflon mold. The film was allowed to form by slow solvent evaporation for 96 h at room temperature. In order to obtain alcohol-treated films the as cast film was immersed overnight in MeOH or EtOH and was dried for 24 h under ambient

conditions. The thickness of the films was determined as an average of at least five points using a digital micrometer (Mitutoyo, model IP6S).

**2.1.1. Thermogravimetric Analysis (TGA).** Thermal stability and the presence of solvent was determined on a Thermal Analysis SDT Q600 device. Before the TGA analysis, the neat powder sample was first refluxed in methanol for 24 h and dried at 120 °C in a vacuum oven (~0.13 mbar) for 6 h. Membrane samples were tested after different conditioning steps in order to reproduce those typically used before the membrane permeability tests. For each experiment, the machine was equilibrated at 25 °C and then the sample was heated to 1000 °C at a rate of 10 °C min<sup>-1</sup>. Measurements were carried out in a N<sub>2</sub> purge flow of 100 mL min<sup>-1</sup>.

**2.1.2. Infrared Spectroscopy (FTIR).** IR analysis of as cast films and MeOH- and EtOH-treated samples was done using a NICOLET 6700 FTIR spectrometer with microscope Continuum (T, R) equipped with DTGS and MCT-A detectors in the range 4000–400 cm<sup>-1</sup>. A total of 64 runs at a resolution of 4 cm<sup>-1</sup> was recorded for each spectrum. Pure liquids were analyzed using a NICOLET iS10 FTIR spectrometer with MCT-A detector in the range of 4000–650 cm<sup>-1</sup> with 16 runs at a resolution of 1 cm<sup>-1</sup> for each spectrum.

**2.1.3. Mechanical Testing.** Tensile tests on the membranes were carried out at room temperature on a Zwick/Roell single column Universal Testing Machine, model Z2.5, equipped with a 50 N load cell and flat grinded steel pneumatic clamps. Specimens with an effective length of 30 mm (distance between the clamps) and a width of 5 mm were tested at a deformation rate of 3 mm min<sup>-1</sup>, corresponding to 10% min<sup>-1</sup>. The average value and the standard deviation of the Young's modulus, the tensile strength and the maximum deformation were determined on a series of 4–6 samples.

**2.2. Gas Permeation Study.** Permeability coefficients were determined for individual gases in three different set-ups, each operating under different conditions (details in Supporting Information).

**2.2.1. Pressure Increase Apparatus.** Single gas permeation measurements were carried out in a fixed volume pressure increase apparatus in the time lag mode,<sup>24</sup> operating with the sample under reduced pressure and having very fast response times.<sup>25</sup> The permeability coefficient,  $P$ , and diffusion coefficient,  $D$ , were determined from the pressure increase rate on the permeate side of the membrane cell assembly in the quasi steady state as described previously.<sup>25</sup> The solubility coefficient,  $S$ , for the gas in the polymer matrix was evaluated indirectly, assuming the validity of the solution-diffusion permeation model with concentration independent transport parameters:

$$S = P/D \quad (1)$$

The ideal selectivity  $\alpha_{A/B}$  for a pair of gases, A and B, was calculated as the ratio of the individual single gas permeabilities,  $P_i$ . It can be decoupled into solubility-selectivity and diffusivity-selectivity:

$$\alpha_{A/B} = \frac{P_A}{P_B} = \frac{S_A}{S_B} \times \frac{D_A}{D_B} \quad (2)$$

**2.2.2. Flow Setup with Gas Chromatographic Analysis.** In the flow setup, with a standard cross-flow cell operating at ambient pressure, with a sweeping gas at the downstream side, the pure gas permeability coefficients were determined by GC analysis of the concentration of the permeating gas in the sweeping gas stream. The partial pressure of penetrants in the downstream part of the cell was negligible, so the penetrants' pressure drops were virtually 1 bar, similar to the time lag setup, but without application of a vacuum on the membrane. The permeability coefficients  $P$  were determined, after establishing a steady-state stream in the cell, by measuring the penetrant concentration in the carrier gas and the total flow of the mixture as described previously.<sup>26</sup>

$$P = \frac{crl}{A\Delta p} \quad (3)$$

where  $c$  is the penetrant concentration in the carrier gas/penetrant mixture (vol %),  $r$  is the flow rate of the gas mixture at the outlet of the cell (cm<sup>3</sup>[STP] s<sup>-1</sup>),  $l$  is the film thickness (cm),  $A$  is the exposed surface area of the film (cm<sup>2</sup>), and  $\Delta p$  is the partial pressure drop of the penetrant across the film (Pa).

**2.2.3. Variable Volume Setup with Mass Spectrometric (MS) Analysis of the Permeate Gas Composition.** Mixed gas permeation tests were carried out in a standard cross-flow cell at a total feed pressure varying from 1 bar up to 7 bar and using helium as a sweeping gas at the permeate side, maintained at atmospheric pressure. The compositions of feed, retentate and permeate were determined with a mass spectrometer (Hiden Analytical) equipped with a quadrupole mass analyzer. The mixed O<sub>2</sub>/N<sub>2</sub> selectivity was evaluated as the ratio of the individually calculated permeances of the gases in the mixture. The individual gas permeance,  $\Pi_i$ , of the  $i$ th species in the ternary mixture is obtained as the ratio of its volumetric permeate,  $Q^{Permeate}$ , to the partial pressure difference between the feed and permeate sides,  $\Delta P_i$ :

$$\Pi_i = \frac{x_i^{Permeate} Q^{Permeate}}{\Delta P_i} = \frac{x_i^{Permeate} Q^{Permeate}}{x_i^{Feed} P^{Feed} - x_i^{Permeate} P^{Permeate}} \quad (4)$$

where  $x_i$  is the mole fraction of the  $i$ th species.  $P^{Feed}$  and  $P^{Permeate}$  are the total feed and permeate pressures, respectively.  $Q^{Permeate}$  is the permeate flow rate per unit area, calculated from the known permeate + sweep flow rate and from the measured composition of the permeate/sweep mixture. With the same procedure the pure CO<sub>2</sub>, N<sub>2</sub>, and O<sub>2</sub> permeabilities were determined as a function of pressure.

**2.2.4. Gas Sorption.** Sorption experiments were performed gravimetrically at 25 °C at gas pressures ranging from 0.5 to 7.5 bar in a home-built sorption apparatus,<sup>27</sup> equipped with a calibrated McBain quartz spiral balance and with automatic charge-coupled device (CCD) camera. The experimental setup and procedure are described in detail elsewhere<sup>28</sup> and in the Supporting Information.

The experimental data were fitted by the dual mode sorption model which describes sorption of gaseous penetrants in glassy polymers:<sup>29</sup>

$$c = k_D p + \frac{C_H b p}{1 + b p} \quad (5)$$

where  $c$  is the sorbate concentration,  $p$  the sorbate pressure,  $k_D$  is the Henry's law constant,  $C_H$  is the Langmuir (monolayer) sorption capacity constant, and  $b$  is the Langmuir affinity constant. Quantitatively, the gas-polymer affinity is best expressed by the factor  $b$  and the infinite dilution solubility,  $S_0$ , which can be calculated from the dual mode parameters:

$$S_0 = \lim_{p \rightarrow 0} \frac{dc}{dp} = k_D + C_H b \quad (6)$$

**2.3. Free Volume Investigation.** The free volume of PIM-EA-TB membranes was investigated by positron annihilation lifetime spectroscopy (PALS) and by <sup>129</sup>Xe NMR spectroscopy.

**2.3.1. Positron Annihilation Lifetime Spectroscopy (PALS).** PALS is based on measurement of lifetimes of positrons in a polymer matrix. The paradigm of the method is an assumption that the longest lifetime in the spectrum, that belongs to hydrogenlike bound state—o-positronium (o-Ps), is related to the size of the mean free volume element (FVE).<sup>29,30</sup> The relationship of the longest lifetimes and the radii of free volume elements is given by Tao–Eldrup equation:<sup>31,32</sup>

$$\tau_i = \frac{1}{2} \left[ 1 - \frac{R_i}{R_0} + \frac{1}{2\pi} \sin \left( 2\pi \frac{R_i}{R_0} \right) \right]^{-1} \quad (7)$$

where  $\tau_i = \tau_3$  or  $\tau_4$  (ns) is o-Ps lifetimes,  $R_i$  is the corresponding radius of a spherical FVE, and  $R_0 = R_i + \Delta R$ , where the adjustable parameter  $\Delta R$  is usually fixed at 1.66 Å. The experimental technique was the same as described earlier.<sup>30,33,34</sup>

**2.3.2. <sup>129</sup>Xe NMR Spectroscopy.** Xenon NMR spectroscopy was performed at 25 °C using a Bruker Avance 500 system with 138.45 MHz <sup>129</sup>Xe resonance, equipped with a 10 mm probe. By setting the gas resonance as reference (0 ppm), and considering the absence of charged ions in the material, the chemical shift of xenon adsorbed by the polymer at vanishing xenon pressure depends only on the physical interactions (collisions) between the Xe atoms and the confining polymer itself.<sup>35</sup> For this case, Demarquay and Fraissard<sup>36</sup> found an empirical relation between the chemical shift and the mean free path  $\lambda$  (expressed in Å).

$$\delta_{Xe} = 243 \left( \frac{2.054}{2.054 + \lambda} \right) \quad (8)$$

The mean free path is a measure of the pore size at least for the analytically solved limiting cases of spherical and cylindrical pores. Because of low sensitivity of the technique at low pressure,  $\delta_{Xe}$  was measured as the intercept of the chemical shifts obtained at several different pressures between 0.2 and 1 bar. Considering the results discussed in section 4.1, PIM-EA-TB was pretreated with methanol before  $^{129}\text{Xe}$  free volume investigation.

### 3. MOLECULAR MODELING

All simulations of the amorphous membrane models were carried out using the Material Studio package (version 5.0) of Accelrys<sup>37</sup> and the PCFF force field.<sup>38</sup>

**3.1. Model Preparation.** A PIM-EA-TB polymer chain of 15 monomer units (653 atoms) was used as template chain for the adjacent initial packing with the Amorphous Cell module. In every packing model, five polymer chains with a total of 3265 atoms were grown together under periodic boundary conditions at 308 K and at an initial density of 0.1 g cm<sup>-3</sup>. Additionally, every simulation cell contained 800 randomly distributed CH<sub>4</sub> molecules as obstacles to avoid ring catenation during the chain growth. The procedure for packing and equilibration are described in detail elsewhere.<sup>39</sup> Amorphous polymer packings were constructed using the Theodorou/Suter method<sup>40,41</sup> as implemented in the Amorphous-Cell module. After equilibration, the NpT-MD simulation was performed at 306 K, pressure of 1 bar for 6 ns. The final density of the models is  $1.03 \pm 0.03$  g cm<sup>-3</sup>. The deviations from the experimental density of 1.08 g cm<sup>-3</sup> is about 5%, which is quite usual for glassy stiff-chain polymer materials, particularly if the models are large.

**3.2. Calculation of Gas Transport Data.** The diffusion ( $D$ ), solubility ( $S$ ), and permeability coefficients ( $P$ ) of H<sub>2</sub>, O<sub>2</sub>, N<sub>2</sub>, CO<sub>2</sub>, and CH<sub>4</sub> were evaluated using the transition state theory (TST) after Gusev and Suter,<sup>42,43</sup> with the programs GSnet and GSdiff.<sup>44</sup> The diffusivity coefficients were determined from the mean square displacement of each gas molecule in the cells, through molecular dynamics simulation runs.<sup>45</sup> These calculations are at the same time a second validation criterion, along with the density, for the quality of the developed packing models. The infinite dilution solubility coefficients were also calculated with the Sorption module in Material Studio. They were obtained from grand canonical Monte Carlo (GCMC) simulations, based on the Metropolis algorithm,<sup>46</sup> by fitting the sorption isotherm obtained from every simulated box to a straight line through the origin and taking the slope to be the solubility coefficient.

**3.3. Free Volume.** The fractional free volume (FFV) and free volume distribution (FVD) were calculated using the Hofmann–Heuchel software.<sup>47</sup> The free volume was determined by first superimposing a fine grid over the cubic packing. Then a spherical test particle, representing the penetrating molecule, was inserted at every point of the grid to determine if an overlap occurs with any atom of the polymer, represented also by a corresponding hard sphere. The result was a classification of grid points as “occupied” or “free”. Then, the connectivity of the “free” grid points was considered, and connected “free” grid points were collected into groups, which represented individual holes. This was done in two ways. In the first approach (named  $V_{\text{connect}}$ ), the topological criterion was that every point of a group had at least one next neighbor, which was also member of this group. This approach identifies holes, which may be of complex shape and of large size. In a second approach, for every grid point, the shortest distance to a polymer atom is used to group points, and, among these distances, local maxima are defined by calculating

the related gradient. Then, each grid point of the free-volume regions is assigned to its nearest local maximum. This approach is referred to as  $R_{\text{max}}$ . The theoretical FVD was compared with that obtained by Bondi’s group contribution method,<sup>48</sup> describing the FFV as the ratio of the free volume,  $V_f$  of a polymer (cm<sup>3</sup> g<sup>-1</sup>) and the specific volume,  $V_{sp}$ , defined as reciprocal density:

$$\text{FFV} = \frac{V_f}{V_{sp}} \quad (9)$$

According to Bondi’s method, the free volume can be estimated as

$$V_f = V_{sp} - 1.3V_{vdW} \quad (10)$$

where the van der Waals volume  $V_{vdW}$  is calculated using a group contribution method, and a universal “packing coefficient”, equal to 1.3, is used to convert the van der Waals volume of the repeat unit into the “occupied” volume.

**3.4. Calculation of Dihedral Angle Distributions.** The structure of the polymer backbone was defined by the dihedral angles between three successive chemical bond vectors. The Cartesian coordinates of the four consecutively bonded backbone atoms forming these bonds were used to calculate the dihedral angle  $\theta$ . The dihedral angle was defined as the smallest angle between the two planes formed by the first three and last three atoms, with the most extended planar (trans) conformation leading to  $\theta = \pm 180^\circ$ .

### 4. RESULTS AND DISCUSSION

**4.1. Thermogravimetric Analysis (TGA).** A PIM-EA-TB powder sample as well as thin films, both as cast and after soaking in different nonsolvents, were analyzed by TGA. The purified powder absorbed approximately 4 wt % of light species, probably air and humidity, which readily desorb below 100 °C. Even after 2 h under vacuum, i.e., under the conditions normally used for conditioning of the membrane before time lag measurements, the as cast membrane still released nearly 20% of residual chloroform between 100 and 300 °C (Figure 1). High affinity with organic species is a characteristic property of PIMs. It is common practice to use alcohol treatment to reset the film casting history of high free volume polymers and to remove the residual solvent.<sup>17,18</sup> The effectiveness of this procedure for PIM-EA-TB was studied systematically using three different fluids for soaking, methanol (MeOH), ethanol (EtOH) and diethyl ether (EtOEt) (Figure 1). Ethanol removes most of the casting solvent (approximately 3% remaining), but in turn appears to be retained itself by the PIM under vacuum until 170 °C. Its presence is confirmed by the intense C–O vibration in the IR spectrum in the range of 1030–1055 cm<sup>-1</sup> (Supporting Information, Figure S1). Diethyl ether completely removes the residual solvent and in spite of its bulkier structure, it remains itself at lower concentration inside the membrane than ethanol. Evidently, lacking the hydroxyl group of ethanol and thus the possibility to form hydrogen bonds with the basic Tröger’s base group, the affinity of diethyl ether for the polymer matrix is smaller. Because of its larger dimensions, it needs a slightly higher temperature than ethanol to be removed (ca. 200 °C). Methanol also removes the casting solvent completely and can be completely removed from the membrane by heating to ca. 95 °C. The C–O vibration in the range of 1030–1055 cm<sup>-1</sup> is missing in the IR spectrum (Supporting Information, Figure S1) of the sample treated with MeOH, proving complete removal of the latter. In addition, after methanol treatment the spectrum of the

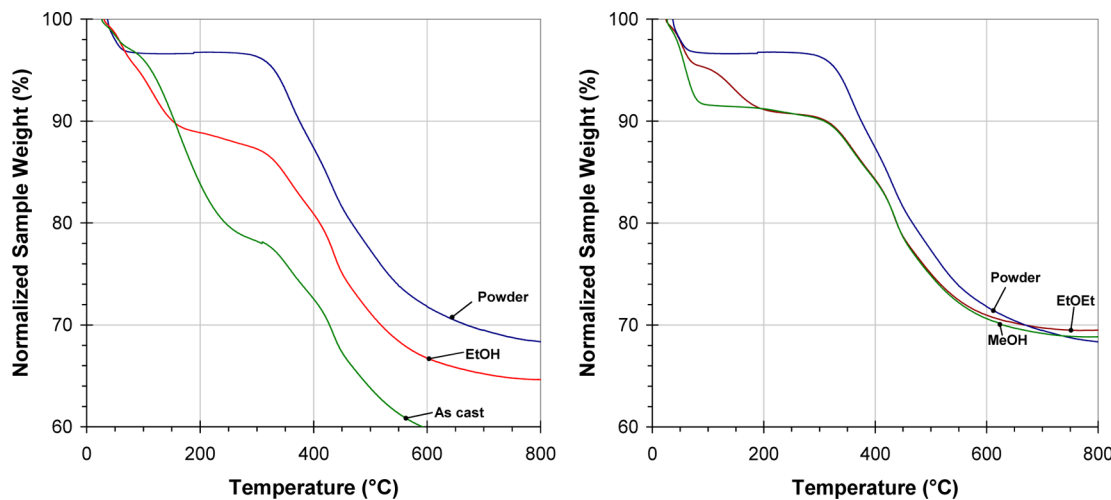


**Figure 1.** TGA curves of PIM-EA-TB samples in  $N_2$  atmosphere. Left: powder sample after reflux in methanol for 24 h and drying at 120 °C in a vacuum oven ( $\sim 0.13$  mbar) for 6 h, as cast membrane and ethanol-treated membrane after 2 h vacuum at 25 °C. Right: PIM-EA-TB powder with diethyl ether-treated membrane and methanol-treated membrane after 2 h vacuum at 25 °C.

polymer changes substantially in the region of 780–640  $cm^{-1}$ . Disappearance of the intense C–Cl bond stretching vibration at 749  $cm^{-1}$  confirms the effective removal of residual chloroform upon methanol treatment.

TGA analysis, in the literature in the range of 25–140 °C indicated that the mass loss of PIM-1 samples cast from chloroform and of samples treated with water was 2.2 and 2.3%, respectively, while the sample treated with MeOH showed a much smaller chloroform content (0.5%). The presence of residual solvent must, at least in part, be ascribed to hydrogen bonding.<sup>19</sup> The much higher amounts of residual casting solvent and absorbed alcohols in PIM-EA-TB with respect to PIM-1 are due to a combination of the higher stiffness of PIM-EA-TB, slowing down desorption of large molecules, and the higher affinity of the organics for the Tröger's base groups in PIM-EA-TB.

For the same type of alcohol and residual solvent, the enhancement of the gas and vapor transport upon post-treatment is much stronger in PIM-EA-TB than in PIM-1 (see below), suggesting a higher increase in the free volume after alcohol soaking of PIM-EA-TB. Interestingly, after soaking in alcohols and subsequent drying, the membrane thickness is up to 10% higher and the diameter is smaller. The casting and subsequent drying procedure

apparently introduces anisotropy into the film, which relaxes upon swelling and plasticization by the alcohol. A similar behavior was observed for Thioamide-PIM-1 membranes upon alcohol treatment<sup>25</sup> and for glassy high free volume perfluoropolymer membranes upon heating above the glass transition temperature.<sup>49</sup>

**4.2. Gas Permeation Parameters.** **4.2.1. Permeability Coefficient.** Samples of PIM-EA-TB with three different molar masses (70, 150, and 190 kDa) were studied using three techniques as is described in the Experimental Section. The samples were tested in the *as cast* state and after alcohol treatment (MeOH and EtOH) and subsequent drying. Table 1 reports the results from time lag measurements and simulated data obtained by the TST method, as well as the results obtained with the cross-flow cell and a sweep gas on the permeate side. Both data for the *as cast* membrane state and for the alcohol-treated samples are given.

Especially the results obtained via the time lag method show that the permeability decreases for all gases with increasing molar mass of the PIM-EA-TB. This trend is less pronounced for the samples after alcohol treatment. In the literature, only few systematic studies have been reported on the transport properties of polymer series with significant differences in their molar mass. The same trend was observed for chitosan membranes.<sup>50</sup>

**Table 1. Permeability Coefficients  $P$  Obtained via a Time Lag Apparatus and by TST Modeling and Selectivities  $\alpha_{ij} = P_i/P_j$  for Various Gas Pairs in PIM-EA-TB Samples with Different Sample Histories**

	sample			$P$ (Barrer) <sup>a</sup>						$\alpha$ (-)				
	state	$M_w$ (kDa)	$L$ ( $\mu$ m)	He	$H_2$	$O_2$	$N_2$	$CO_2$	$CH_4$	He/ $N_2$	$H_2/CH_4$	$O_2/N_2$	$CO_2/N_2$	$CO_2/CH_4$
time lag setup		70	178	779	2175	687	178	2319	259	4.39	8.40	3.87	13.05	8.95
	as cast	150	152	223	568	259	76	1400	152	2.92	3.74	3.39	18.34	9.23
		190	87	219	517	205	63	1022	131	3.47	3.95	3.24	16.18	7.80
	EtOH	61	141	2320	6450	1430	300	3690	340	7.80	18.73	4.81	12.41	10.72
	MeOH	70	182	2570	7760	2150	525	7140	699	4.90	11.11	4.10	13.6	10.21
	MeOH	190	91	2676	7069	1510	334	7696	488	8.02	14.49	4.53	13.70	15.77
flow cell <sup>b</sup>	as cast, GC	70	122	345	880	365	112	2010	254	3.1	3.5	3.3	17.9	7.9
	MeOH, MS	70	129	—	—	1592	365	6918	—	—	—	4.4	19.0	—
	EtOH, GC	70	211	1849	5460	2390	780	11325	1160	2.4	4.7	3.1	14.5	9.8
	EtOH, GC	190	196	1088	3383	1237	457	6883	964	2.4	3.5	2.7	15.1	7.1
TST				8434	2451	692	517	1192		7.1	3.54			

<sup>a</sup>1 Barrer =  $10^{-10}$   $cm^3 cm cm^{-2} s^{-1} cmHg^{-1}$  =  $3.35 \times 10^{-16}$  mol  $m m^{-2} s^{-1} Pa^{-1}$  <sup>b</sup>GC = gas chromatographic method, MS = mass spectrometry method with pure gas.

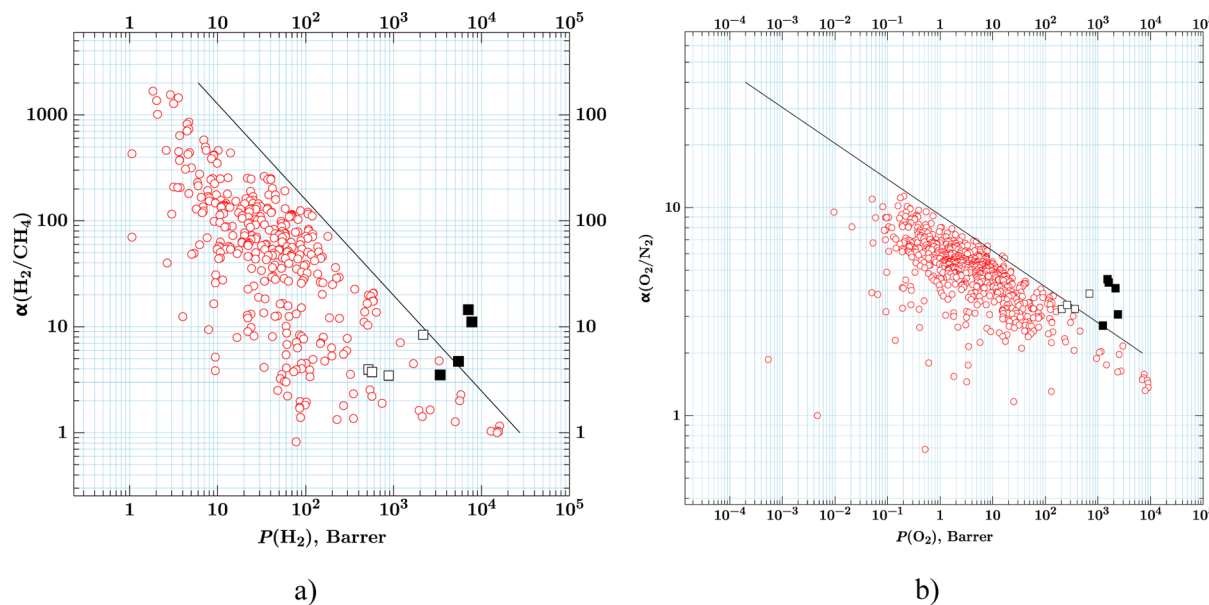


**Figure 2.** Robeson's diagrams: (a) H<sub>2</sub>/CH<sub>4</sub> gas pair; (b) O<sub>2</sub>/N<sub>2</sub> gas pair. The line represents the upper bound of 2008.<sup>9</sup> The red data points are taken from The Database.<sup>54</sup> Open squared symbols: as cast PIM-EA TB. Filled squared symbols: alcohol-treated samples of PIM-EA-TB.

Indeed, in relatively densely packed polymers the end groups have greater mobility and in short chains they should contribute to a higher free volume, facilitating gas diffusion. However, in monodisperse polystyrenes the solubility coefficients were found to increase with increasing  $M_w$ .<sup>51</sup> For an analogous series of PIM-1 samples, a decrease of permeability with increasing molar mass was also found.<sup>52</sup>

Indeed, in PIMs the situation is more complex, since the high FV is related to the lack of freedom of motion and contorted chain structure with poor packing. Therefore, the effect of end groups is not unambiguous, because increased mobility might also lead to more efficient packing and lower free volume. In PIM-1, it was observed<sup>52</sup> that a higher MW often implies a higher degree of branching. Since branch points contribute to a higher local density they lead to a decrease in FV and a decrease in permeability. The net effect of the end groups and the branch points may be uncertain, but in the present case of PIM-EA-TB, the overall effect of increasing molar mass is a decrease in permeability. This is in contrast with what happens in relatively densely packed polymers, where (hyper)branching is used as a strategy to increase permeability: the free volume increases by the increased mobility of the relatively high number of end groups, while the branch points disturb possible order and decrease the packing efficiency.<sup>53</sup>

Table 1 shows considerable differences between individual measured values of the permeability coefficients. The  $P_i$  values differ by a factor of 2–3, well beyond statistical errors of the measurements. It can be ascribed only in part to the different boundary conditions of different methods, which were almost the same in TL, GC, and MS methods: 1 bar upstream and ca. zero partial pressure in the downstream parts of the setups (for MS and GC, the sweep is at a pressure of 1 bar). Nevertheless, a slight influence of the sweeping gas itself cannot be excluded due to its back-diffusion from the permeate to the feed side. Thus, the scatter in the values of  $P_i$  can be related to the different states of the membranes, different boundary conditions and/or to an uncontrolled degree of aging that can be very high in some extreme conditions. The transport of smaller gas molecules is preferred to the larger molecules, indicating a somewhat different

trend than in PIM-1, because of a stronger size sieving nature of PIM-EA-TB.<sup>10</sup> The largest reduction in permeability with respect to PIM-1 is observed for CO<sub>2</sub>. In PIM-1, CO<sub>2</sub> is the gas with the highest permeability coefficients, while in PIM-EA-TB, H<sub>2</sub> has  $P$  values comparable with those of CO<sub>2</sub>. The large enhancement of permeability of alcohol-treated PIM-EA-TB, by a factor of 5–12 (depending on the samples and method used) is much stronger as compared with PIM-1, where permeability increased only 3-fold.<sup>5</sup>

The simulated data of gas permeability in PIM-EA-TB (Table 1) confirm the trend of the experimental data. The absolute values are closer to the experimental permeability of the unaged treated membranes because the polymer structure reproduced by modeling is “empty” as obtained just after alcohol treatment. Zhou et al. estimated higher permeability for the same polymer, the difference owing to the lower density of their models.<sup>53</sup>

It is common to assess the permselectivity of membranes using the Robeson diagrams,<sup>9,13</sup> where every polymer structure is characterized by a single point. However, since different samples of PIM-EA-TB showed different transport parameters, several data points appear in Robeson diagrams (Figure 2). In some cases, selectivity decreases with increasing permeability, while in numerous cases selectivity increases with increasing permeability. Interestingly, among these points no classical trade-off between  $P_i$  and  $\alpha_{ij}$  is observed, indicating that different techniques assess the transport properties differently. Anyway, the majority of the data points of PIM-EA-TB are above the upper bound of 2008.<sup>9</sup> The separation factors show smaller variations than the permeability because of partial compensation of variations of the permeability values in the numerators and denominators (eq 2), which generally move into the same direction.

**4.2.2. Diffusivity and Solubility.** The gas transport in PIM-EA-TB was analyzed considering the solution-diffusion model. According to this model, both, the diffusion coefficient  $D$  and the solubility  $S$  (Table 2) were evaluated. Computer modeling furthermore provided an estimation of the solubility coefficients using TST and GCMC approaches and diffusion coefficients were computed using TST and MD methods. Both data sets are plotted in Figure 3 as correlations of  $\log D$  versus  $d^2$  and  $\log S$

**Table 2.** Experimental and Computational Gas Diffusion and Solubility Coefficients in PIM-EA-TB Samples with Different Sample Histories<sup>a</sup>

state	$M_w$ (Da)	$L$ ( $\mu\text{m}$ )	sample								S ( $\text{cm}^3 (\text{STP}) \text{cm}^{-3} \text{bar}^{-1}$ ) <sup>b</sup>							
			He	$\text{H}_2$	$\text{O}_2$	$\text{N}_2$	$\text{CO}_2$	$\text{CH}_4$	He	$\text{H}_2$	$\text{O}_2$	$\text{N}_2$	$\text{CO}_2$	$\text{CH}_4$				
as cast	70k	178	>5028	>2986	125.5	36.2	38.6	12.9	<0.12	<0.55	4.11	3.68	45.07	15.12				
	150k	152	(409)	(349)	77	35.7	40.3	22	(0.41)	(1.22)	2.52	1.61	26.03	5.17				
n.a. <sup>c</sup>	144										1.99	1.07	31.67	8.41				
190k	87	>2000	>1200	68.2	25.3	22.8	9.94	<0.07	<0.3	2.25	1.88	33.68	9.88					
MeOH	70k	182	>10000	>7000	31.8	99.5	87.0	36.0	<0.2	<0.8	6.0	4.7	57.0	14.8				
	190k	91	>6000	>5000	31.0	89.3	87.3	31.9	<0.3	<1.1	7.26	7.21	83.95	35.14				
MD (TST)		—	11300 ± 50	227 ± 5	79 ± 3	1.4 ± 0.4	28 ± 5	—	0.563 ± 0.38	8.25 ± 3.0	6.60 ± 2.25	283 ± 1.5	32.25 ± 5.25					
MD		19700 ± 30	9790 ± 70	150 ± 50	42 ± 6	7 ± 3	6 ± 3	—	0.30 ± 0.53	2.48 ± 0.23	4.20 ± 0.53	24.0 ± 1.50	6.15 ± 0.68					

<sup>a</sup>Experimental data obtained from a time lag apparatus. <sup>b</sup> $b_1$  ( $\text{cm}^3(\text{STP}) \text{cm}^{-3} \text{cmHg}^{-1}$ ) = 75.006 ( $\text{cm}^3(\text{STP}) \text{cm}^{-3} \text{bar}^{-1}$ ). <sup>c</sup>Data obtained from sorption kinetics. Different polymer batch.

versus  $T_c$ , where  $d$  is the kinetic cross section diameter according to Teplyakov and Meares<sup>55</sup> and  $T_c$  is the critical temperature of the gases. Comparison of PIM-EA-TB data with those of PIM-1 are also shown.

Several conclusions can be drawn from these plots and from a comparison with corresponding data for PIM-1.

- (1) The  $D$  and  $S$  values of PIM-EA-TB are rather similar to those of PIM-1. Budd et al.<sup>5</sup> claimed that the gas solubility coefficients of PIM-1 are higher than those of all studied polymers. It is obvious that PIM-EA-TB is another solubility champion with extremely high solubility coefficients for  $\text{CO}_2$ . On the other hand, in PIM-EA-TB the  $\text{CO}_2$  diffusivity is relatively slow in comparison with PTMSP and various other highly permeable polymers: the presence of two basic nitrogen atoms in the PIM-EA-TB backbone increases the interaction with  $\text{CO}_2$ , slowing down its diffusion.<sup>56</sup>
- (2) Methanol treatment of PIM-EA-TB results in strong, 2–3-fold increase in the diffusivity. In the case of PIM-1, this effect is approximately the same.<sup>5</sup> Diffusivity of small gases is higher in PIM-EA-TB than in PIM-1. The difference becomes smaller or is reversed with increasing gas molecular dimensions, indicating the stronger size sieving behavior of PIM-EA-TB.<sup>10</sup>
- (3) With respect to PIM-1, there is a modest increase of solubility in PIM-EA-TB after methanol treatment.
- (4) The comparison between theoretical and experimental diffusivity indicates a similar trend. Calculated diffusivity of small gases is higher in PIM-EA-TB than in PIM-1 and is equal or reversed with increasing gas molecular dimensions. The diffusion coefficients in PIM-EA-TB are in agreement with experimental data and are higher than that of PIM-1 for smaller gases and are in the between the calculated data of PIM-1 for larger gases: lower than those of MD,<sup>57</sup> but higher than those of TST.<sup>39</sup> The exception is  $\text{CO}_2$  diffusivity that is underestimated by simulation, both with MD simulation runs and with TST method. In the literature, it has been reported that predictions are much less reliable for diffusion coefficients than for solubility, and it is commonly accepted that if the  $D_{\text{theoret}}$  and  $D_{\text{exp}}$  values differ by a factor of 2–5, then the prediction is considered to be successful.<sup>58</sup> Therefore,  $\text{CO}_2$  has been excluded on the right diffusivity-plot (Figure 5b). The exception of  $\text{CO}_2$  is not surprising: Heuchel et al. already mentioned this limitation for TST results for PIM-1<sup>39</sup> and for polyimides,<sup>59</sup> for which calculated diffusion coefficients are about 1 order of magnitude too small, whereas the calculated solubilities are higher than the experimental values. The general explanation is related to the anisotropy of  $\text{CO}_2$  and its strong interaction (not well represented by the Lennard-Jones parameters), and to the missing “relaxational” motions of the matrix in the TST method. The  $S$  values simulated using GCMC are in reasonable agreement with experimental solubility coefficients up to oxygen then is underestimated. TST method gives the best comparison with larger gases with the well-known deviation for  $\text{CO}_2$ . The two methods give similar values and trends, independently on the polymers. The relatively small dimension of the boxes does not permit a very high statistic to be reached, but considering that the accuracy of the predictions of the  $S$  values is sensitive to the appropriate choice of the force field (see, e.g., refs 58 and 60), the simulation results are reliable enough for further discussion in this paper.

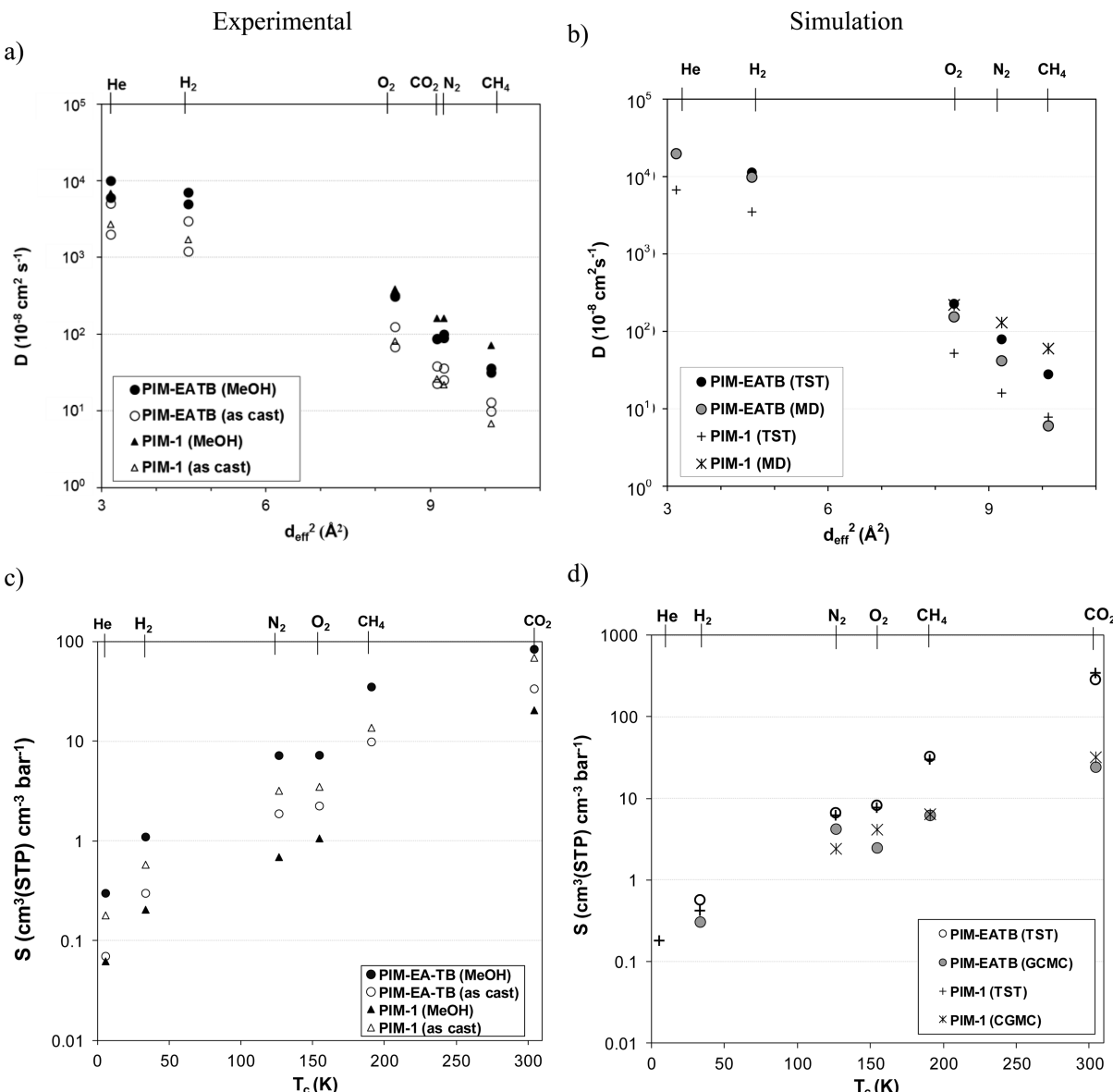


**Figure 3.** (a, b) Correlation of the diffusion coefficients with the squared cross-section diameter of penetrants for PIM-EA-TB. (c, d) Correlation of the solubility coefficients with the critical temperature of penetrants for PIM-EA-TB. Left: experimental values of PIM-EA-TB (190 kDa). Right: data from simulations. Data for PIM-1 are shown for comparison (experimental,<sup>5</sup> TST,<sup>39</sup> and MD values<sup>57</sup>).

**4.2.3. Gas Sorption.** Sorption isotherms of independent gas sorption measurements at 25 °C are concave to the pressure axis as it should be in sorption in glassy polymers (Figure 4). Both the as cast samples and especially the methanol-treated samples of PIM-EA-TB showed notably higher gas uptake than the archetypal PIM-1 polymer. The experimental data were fitted with the dual mode equation (eq 5). Infinite dilution solubility coefficients as well the solubility coefficients at 1 bar are listed in Table 3. For nitrogen, in the as cast samples, a linear fit was used because the pressure range was too narrow to have sufficient curvature. For the same reason, also for methane in the as cast samples and for nitrogen in the methanol-treated samples, the fit should be interpreted qualitatively, rather than quantitatively.

The initial slope of the CO<sub>2</sub>, CH<sub>4</sub>, and N<sub>2</sub> sorption isotherms is significantly higher for methanol-treated PIM-EA-TB than for methanol-treated PIM-1, whereas it is almost equal for the nontreated samples. The increase of gas sorption in

methanol-treated PIM-EA-TB is most significant for CO<sub>2</sub> and the bulkier CH<sub>4</sub> molecules. This suggests that the methanol treatment opens up a fraction of the free volume, which would otherwise be inaccessible to these gases. The high infinite dilution selectivity for CO<sub>2</sub> confirms the much stronger interaction of CO<sub>2</sub> with the PIM-EA-TB polymer matrix as compared to N<sub>2</sub>. This is qualitatively shown by the extremely steep start of the CO<sub>2</sub> sorption isotherm. Similar strong affinity of CO<sub>2</sub> with the polymer matrix was recently reported for Amine-PIM-1<sup>56</sup> and is related to the presence of primary amine groups in Amine-PIM-1 and to the tertiary amines in the Tröger's base in the present PIM-EA-TB. As cast PIM-EA-TB shows a clearly higher CO<sub>2</sub>/N<sub>2</sub> (26) and CO<sub>2</sub>/CH<sub>4</sub> (4) sorption selectivity at 1 bar than PIM-1 (9.4 or 3.5, respectively). After MeOH treatment, due to a significantly higher nitrogen sorption, the corresponding CO<sub>2</sub>/N<sub>2</sub> and CO<sub>2</sub>/CH<sub>4</sub> sorption selectivity dropped to 11 and 2.8, respectively, for PIM-EA-TB, and to 15.5 and 3.0, respectively for CO<sub>2</sub>/N<sub>2</sub> and CO<sub>2</sub>/CH<sub>4</sub> in PIM-1.

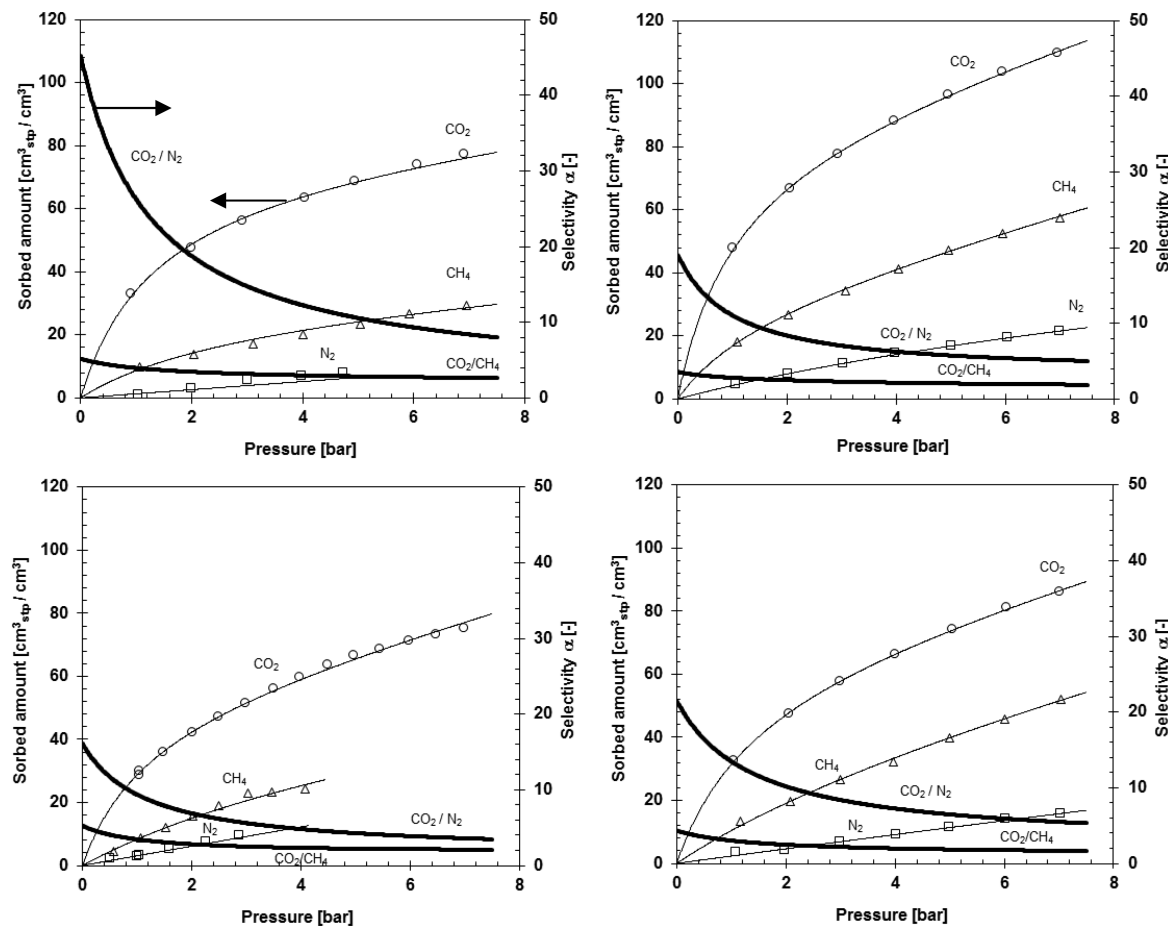


**Figure 4.** Gravimetric sorption isotherms at 25 °C for CO<sub>2</sub> (O), CH<sub>4</sub> (Δ) and N<sub>2</sub> (□) in *as cast* PIM-EA-TB (top-left), MeOH-treated PIM-EA-TB (top-right) and *as cast* PIM-1 (bottom-left) and MeOH-treated PIM-1 (bottom-right) membranes. Thin solid lines (left axis) represent the fit of the data according to the dual mode sorption model (eq 5). Thick solid lines (right axis) represent the corresponding ideal sorption selectivity calculated from the dual mode sorption curve fit.

**Table 3. Infinite Dilution Solubility Coefficients  $S_0 = k_D + C_H b$  Obtained from a Least-Squares Fit of the Sorption Isotherms in Figure 4, and Solubility Coefficients at 1 bar ( $S_1$ ) of As Cast PIM-EA-TB and PIM-1 Samples<sup>a</sup>**

gas	polymer	$S_0$ , cm <sup>3</sup> (STP) cm <sup>-3</sup> bar <sup>-1</sup>	$S_1$ , cm <sup>3</sup> (STP) cm <sup>-3</sup> bar <sup>-1</sup>	source
CO <sub>2</sub>	PIM-EA-TB	58.8 (87.5)	34.1 (46.9)	this work
	PIM-1	49.3 (50.4)	28.7 (31.4)	this work
		47.0	—	61
CH <sub>4</sub>	PIM-EA-TB	11.3 (24.5)	8.63 (16.8)	this work
	PIM-1	9.4 (11.6)	8.32 (10.4)	this work
		10.3	—	61
N <sub>2</sub>	PIM-EA-TB	1.3 (4.6)	1.3 (4.24)	this work
	PIM-1	3.06 (2.3)	3.06 (2.33)	this work
		2.85	—	61

<sup>a</sup>Values for MeOH-treated samples are given between parentheses.

It must be noted that there is a significant discrepancy between the sorption data in Table 3 and the indirectly determined solubilities in Figure 3. This is due to anomalous transport. In particular, for readily condensable gases such as CO<sub>2</sub>,<sup>56,61</sup> pressure dependence of  $P$  and  $D$  generates a nonlinear concentration profile across the membrane and thus incorrect indirect calculation of the solubility from  $S = P/D$ . Similar discrepancies have been described by K. Friess et al., using three different methods to study vapor transport in polyethylene.<sup>28</sup> The most fundamental difference is that the transient curve in the permeation measurements reflects the phenomena at the low pressure (low

concentration) side of the membrane, whereas the transient in sorption experiments reflects the phenomena at the high pressure (high concentration) side of the membrane. These phenomena are fundamentally different in the case of gases with pressure dependent transport parameters.

**4.2.4. Transport Anomalies.** From the above, it becomes evident that the transport parameters strongly depend on the sample history and on the specific measurement technique. Previously, it was found for a number of freshly prepared PIMs that under otherwise comparable conditions of 1 bar feed pressure and negligible partial pressure in the permeate (with vacuum for the time-lag method and

sweep gas for the variable volume method in the cross-flow cell) freshly soaked membranes exhibited systematically lower permeabilities in the time lag instrument than in the variable volume setup. Similar scatter in the results is found for many polymers in the literature, for instance for different samples of PTMSP<sup>20</sup> or PEI,<sup>34</sup> but this phenomenon has rarely been discussed systematically. Since PIMs seem to be particularly sensitive, due to the strong sorption of vapours in these highly porous polymers,<sup>64</sup> the effect of the two most important variables, pressure and time, were further studied.

Figure 5 shows the pure gas permeability of a freshly alcohol-treated membrane as a function of the feed pressure in the

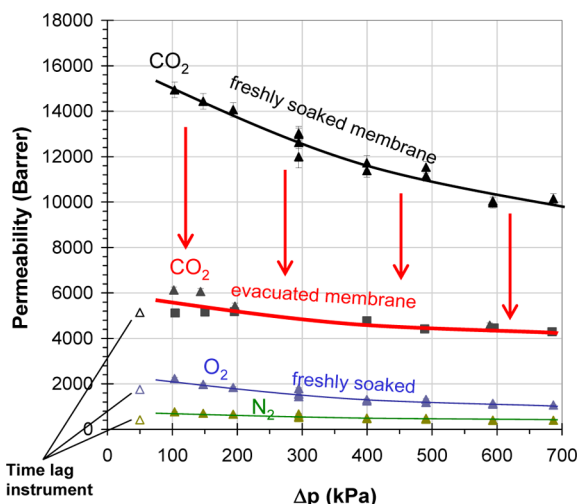


**Figure 5.** Permeability of pure CO<sub>2</sub> (black), O<sub>2</sub> (blue), and N<sub>2</sub> (green) gases measured on a MeOH-treated PIM-EA-TB membrane as a function of the feed pressure in the cross-flow cell. The corresponding data determined by the time lag method are given as triangles ( $\Delta$ ) at  $\Delta p = 0.50$  kPa, the average between feed and permeate pressure. The red curve indicates the decrease in CO<sub>2</sub> permeability of the membrane after the analysis in the time lag instrument.

cross-flow cell, using helium as a sweep gas. The permeability slightly decreases with pressure. This is in good agreement with

the observed dual mode behavior and is typical for glassy polymers. It depends on the decreasing solubility coefficient by saturation of the Langmuir sorption sites at higher pressures. The permeability determined by the time lag instrument, given for comparison, appears to be much lower, especially for CO<sub>2</sub>. Interestingly, a second test under the same conditions showed that the CO<sub>2</sub> permeability decreased irreversibly by vacuum treatment during the measurement in the time lag instrument. This decrease was identified as the main reason for the systematic discrepancy between the permeabilities of freshly alcohol-treated membranes obtained by the two methods. The vacuum in the time lag instrument apparently changes the membrane properties as compared to samples which have never been exposed to a vacuum. In part, this may be related to humidity, absorbed from the air. Unreported experiments indicated that a sample which is repeatedly measured over a long time interval ages faster; i.e., its permeability decreases faster, compared to an identical sample which is tested only at the beginning and at the end of that time interval.<sup>63</sup> It is hypothesized that the repeated removal and absorption of humidity helps the sample to approach the thermodynamic equilibrium state.

The origin of this anomalous behavior is further illustrated in Figure 6, showing the permeability of a freshly methanol-treated and air-dried membrane as a function of time during permeation of pure CO<sub>2</sub>. The inline mass spectrometric analysis of CO<sub>2</sub> in the permeate allows a detailed evaluation of the early stage permeation process from the very first exposure of the membrane to CO<sub>2</sub>. After the start of the experiment there is an initial increase in the permeate flux from ca. 0.1 to ca. 0.2 h, which approximately corresponds to the expected time scale of the permeation transient. Before leveling off, the permeability then suddenly increases further and stabilizes at ca. 18000 Barrer after 0.5 h, where it remains stable until approximately 1.5 h. This increase takes much longer than would be expected on the basis of the time lag measurements, and corresponds to the CO<sub>2</sub>-induced removal of the residual methanol, which is still present according to the TGA analysis in Figure 1. At 4 bar (absolute) the sample absorbs more than 15 wt % of CO<sub>2</sub> (Figure 4). This is expected to promote the removal of the trapped methanol by

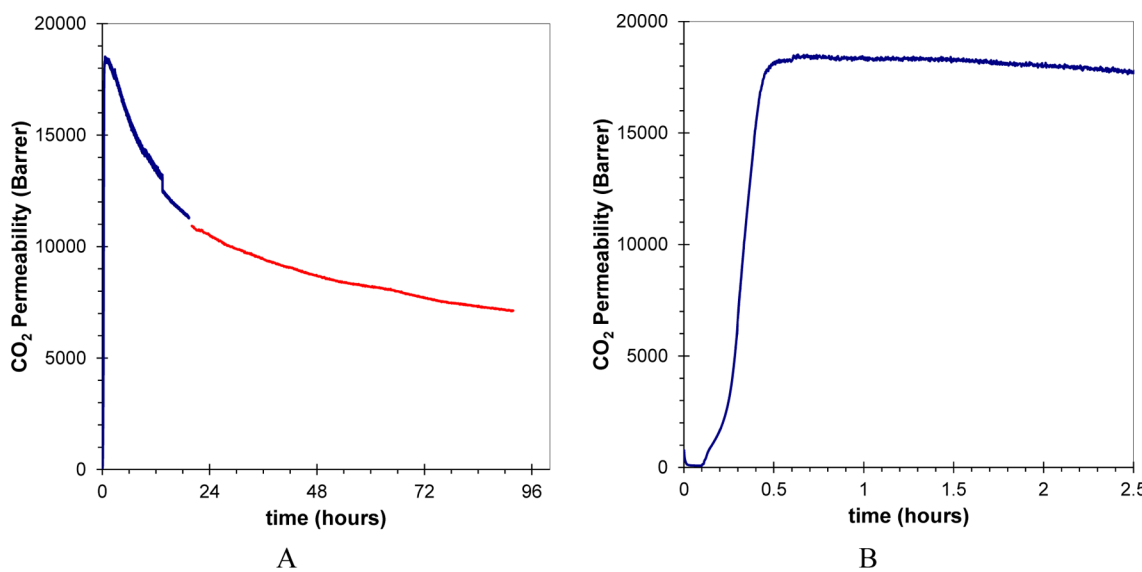


**Figure 6.** (A) Carbon dioxide permeability through a PIM-EA-TB membrane as a function of time at 3 bar in the cross-flow cell by the variable volume method. (B) Zoom of the first 2.5 h, allowing observation of the transient behavior. The initial flat signal is because the analyzer was switched on before exposure of the membrane to CO<sub>2</sub>.

**Table 4. Parameters of Positron Annihilation Lifetime Spectroscopy for PIM-EA-TB and other High Free Volume Polymers, Including Time Dependence of the  $\tau_4$  Parameter for PIM-EA-TB<sup>a</sup>**

polymer	conditions		$\tau_3$ , ns	$I_3$ , %	$\tau_4$ , ns	$I_4$ , %	$R_3/R_4$	ref
	N <sub>2</sub>	0 days						
PIM-EA-TB	air	0 days	1.66	8.3	5.70	24.2	2.52/5.07	this work
		1 day			4.35 ± 0.09			
		3 days			4.40 ± 0.11			
		9 days			4.26 ± 0.08			
PIM-1	N <sub>2</sub>	0 days	2.13	6.1	5.81	17.8	2.97/5.11	5
additive Si-containing polytricyclononene	N <sub>2</sub>	0 days	2.65	10.7	10.1	28.0	3.39/6.59	66

<sup>a</sup>Similar values of lifetime were reported by Lima de Miranda et al.<sup>67</sup>

the double action of CO<sub>2</sub>: swelling of the polymer matrix that facilitates methanol diffusion, and competitive sorption, actively displacing methanol from the sorption sites. Interestingly, a reduction of the permeability sets in after a stable period of several hours. Since the typical duration of permeability measurements with individual gases is not more than 30 min, this change is generally not seen, or not reported. At much longer times, the membrane shows approximately a 2-fold reduction of the permeability during the first 24 h and the permeability continues to decrease at a much lower rate over longer times. Apparently, the vacuum treatment of the sample in the time lag instrument drastically accelerates this process and causes the permeability in this instrument to be systematically lower than the permeability in the variable volume method.

**4.3. Free Volume Analysis: Experimental Determination.** **4.3.1. PALS.** The results of the PALS study of PIM-EA-TB are presented in Table 4. The lifetime spectrum comprises two o-Ps lifetimes ( $\tau_3$  and  $\tau_4$ ), which is a feature of highly permeable polymers like poly(trimethylsilyl propyne) or amorphous Teflons.<sup>20</sup> This result is in agreement with the high permeability of PIM-EA-TB, as discussed before. Measurements in contact with air resulted in some shortening of o-Ps lifetimes due to the oxygen quenching, another feature of highly permeable polymers or sorbents.<sup>65</sup> The radii of FV elements in this polymer calculated via the Tao–Eldrup equation are rather similar to those found for PIM-1, especially as concerns  $R_4$ . The  $R_3$  value observed for PIM-EA-TB is smaller than that for the corresponding PIM-1  $R_3$ . Another polymer taken for comparison, poly(tricyclononene) containing two SiMe<sub>3</sub> groups<sup>66</sup> shows somewhat longer lifetimes and larger radii  $R_3$  and  $R_4$ . This is consistent with its greater permeability. As discussed, time dependence of the transport parameters is a characteristic for PIM films. Therefore, the PALS parameters for PIM-EA-TB were checked periodically during more than 1 week. Measurements were performed in air atmosphere. The results presented in Table 4 indicate no significant changes in time in the observed  $\tau_4$  lifetime. Hence, any variations of the transport parameters should be interpreted as not due to the changes of the size of FVEs but more probably due to changes in the connectivity of free volume.

**4.3.2. <sup>129</sup>Xe NMR.** <sup>129</sup>Xe NMR spectroscopy was carried out as an independent characterization of the average free volume element size and connectivity. Spectra acquired in the presence of methanol-treated PIM-EA-TB show two resonance signals: one upfield due the free gas phase and one corresponding to the gas absorbed by the polymer (Supporting Information, Figure S2). The signal ratio reveals significant xenon sorption in the polymer, while the free gas peak is slightly above the noise level. At 108 kPa nominal pressure, uptake can be estimated as

≥90% of the original gas present, i.e. approximately 30 mg of gas is absorbed by 179 mg of sample.

The chemical shift measured at variable pressure between 20 and 108 kPa (Supporting Information, Figure S2) could be fitted ( $R^2 > 0.99$ ) linearly, with a back extrapolated  $\delta_{\text{Xe}}$  value of 109.7 ppm at zero pressure. Equation 8 then yields a mean free path of 2.50 Å, corresponding to spherical micropores of 4.70 Å radius or cylinders with a radius of 3.45 Å. In comparison, <sup>129</sup>Xe spectra of PIM-1 reported a shift around 132 ppm at 50 kPa<sup>68</sup> as well as regions of non linearity over 100 kPa that suggested us to work at lower pressures. The line width of the peak attributed to gas interacting with PIM-EA-TB is small as compared to xenon exploring natural materials,<sup>69</sup> but much wider than in PIM-1 (740 Hz vs 280 Hz at 1 atm). This result, independent of pressure, indicates a greater variety of probed environments with the presence of many sites that xenon can explore within the NMR acquisition time scale (few milliseconds) due to high connectivity of the pore system.

**4.4. MD Simulations.** **4.4.1. Fractional Free Volume (FFV).** The fractional free volume of PIM-EA-TB, simulated using the conventional Bondi method, was found to be 0.276, which is just slightly larger than the value of 0.24–0.26, estimated by Guiver et al. for PIM-1, using van Krevelen's group contribution method.<sup>48</sup> The free volume is often correlated with the permeability of membranes,<sup>70</sup> and the high FFV found for PIM-EA-TB is in good agreement with its high permeability. However, this number alone is insufficient to explain the high selectivity for certain gas pairs. In fact, the main limitation of Bondi's method, PALS, and <sup>129</sup>Xe NMR, or of any other experimental probing method, is that these methods only give the total free volume or an indication of the average free volume element size. These may correlate with permeability, but as an explanation of the full set of transport properties, this is not sufficient. In particular, these methods fail to provide any information regarding the connectivity of the free volume.

The enormous advantage of computational methods is that they can give much more information on the free volume size distribution, and even on the spatial arrangement of the free volume.<sup>71</sup> For the analysis of the size distribution of the free volume elements in PIM-EA-TB, three packing models were constructed. Thin slices, cut along the z-direction of a representative 3D cell of PIM-EA-TB are displayed in Figure 7. The empty regions between the atoms give a qualitative indication of the free volume elements. The FVE sizes are rather large and an irregular structure is visible, with FVE elements elongated through two or three slices, as in PIM-1.<sup>47</sup> The insert gives an alternative representation, showing even better the presence of both very large and small voids, as well as narrow connections between the larger voids.

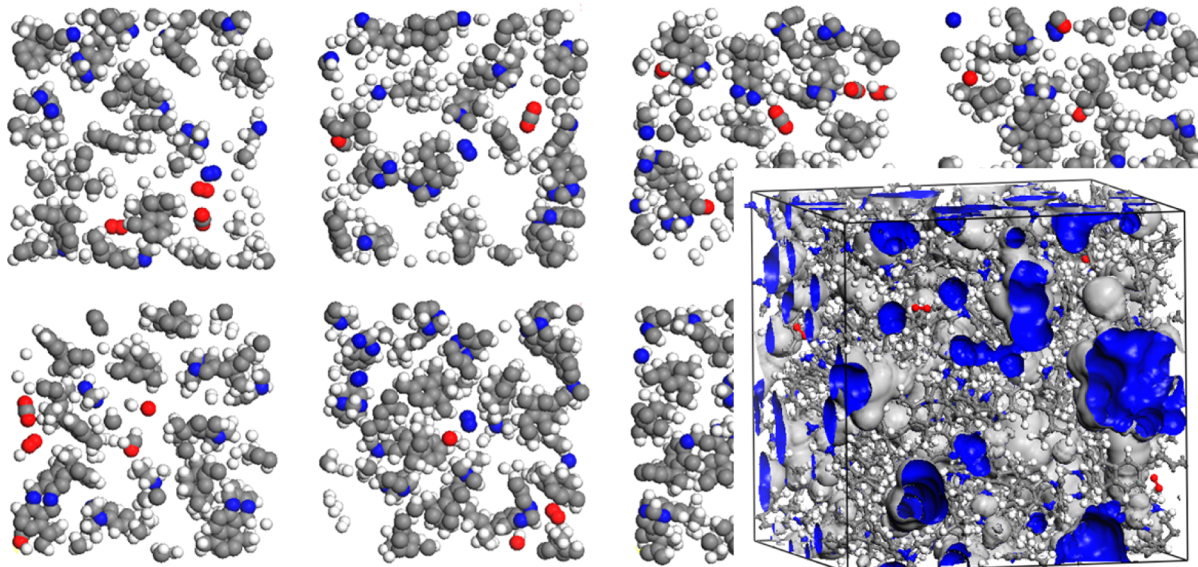


**Figure 7.** Model of PIM-EA-TB showing slices of about 4.2 Å across z axes, with voids given as empty space. A limited number of gas molecules ( $\text{N}_2$ ,  $\text{O}_2$ ,  $\text{CO}_2$ ) are present in the voids. Red for oxygen, blue for nitrogen, white for hydrogen and gray for carbon atoms. The inset shows a 3D model, evidencing the free volume elements as gray bubbly shapes. FVEs crossing the box boundary allow an inside view and are highlighted with a blue inner coating. Length of the box edges: 34 Å.

**4.4.2. Analysis of the Free Volume Element Size Distribution.** As outlined above, the gas transport behavior is affected by the overall free volume and by its morphology or connectivity. To investigate the FV morphology, the Hofmann–Heuchel method was employed.<sup>47</sup> This method gives qualitative and quantitative indications on the dimensions of holes and the possible interconnectivities (Figure 8A). The free volume element size distribution was quantified by the  $R_{\max}$  and  $V_{\text{connect}}$  approach for three equilibrated packing cells of PIM-EA-TB, setting the probe radius to the size of an o-positronium particle (radius = 1.1 Å) and using a grid spacing of 0.5 Å. This approach to analyze the distributions of fractional free volume elements accessible for an o-positronium probe, is generally used for immediate comparison with PALS data.<sup>72,73</sup> Thus, Figure 8A shows the free volume size distributions as an average of the three PIM-EA-TB packing models, using a positronium probe, while PALS and NMR data are given for comparison. The  $V_{\text{connect}}$  distribution shows peaks for equivalent spheres with apparent “radii” in a range up to about 15 Å which is in the same range found also for other high performance polymers.<sup>39,72–74</sup> It should be emphasized that such radius does not imply that the packing model contains a single huge spherical hole of this size, but it indicates only the measure of the total extension of an interconnected free volume region. PIM-EA-TB shows the typical bimodal cavity size distribution frequently observed for high free volume materials. I.e., they have two qualitatively different free volume phases: one composed of relatively small isolated holes where the free volume distribution resembles that of conventional glassy polymers, and one of highly interconnected micropores, which provide the exceptional diffusion pathways. The comparison with PIM-1 (ref 39 and Supporting Information, Figure S3) indicates a similar distribution of voids with a number of intermediate-sized and fewer extremely large highly interconnected voids in the PIM-EA-TB as the main difference. The FVEs in PIM-EA-TB calculated via the  $R_{\max}$  approach show a continuous distribution within 5 Å, and the  $V_{\text{connect}}$  approach shows additional distinct shoulders at cavity radii of about 10 Å plus a larger peak around 15 Å. The geometrical splitting of larger free volume regions into smaller parts obviously

increases the number of pores (holes) considerably. The maximum of the  $R_{\max}$  distribution is at about 2.6 Å, very similar to the value obtained from the average of the integration of the  $R_{\max}$  distribution. It also agrees well with the PALS results, including both peaks from the PALS experiments, with a superposition of the small radius (of 2.52 Å) with the average  $R_{\max}$  peak. The FVE size distributions of PIM-1 show a continuous distribution of peaks up to 6–8 Å and then larger volume elements at about 17 Å.

A comparison of the main results from the different techniques is given in Table 5. The mean FVE sizes from all experimental and theoretical techniques are in between the peak maxima from the PALS data. The simulation results are almost the same as the PALS ( $R_3$ ) result, whereas the  $^{129}\text{Xe}$  NMR data are closer to the larger  $R_4$  radius. The agreement between the various experimental methods and between the experimental versus computational method is reasonable. Each of the used methods “senses” the free volume in another specific way, with probes of different size and properties, and each method provides a different level of detail in the obtained results. PALS allows the best experimental probing of the FVE distribution due to the small size of the o-Positronium particles, but in contrast to the MD simulations it can only probe the volume and to some extent the shape, but not the connectivity of the FVEs. Simulation remains, therefore, the most powerful method to analyze the free volume.

**4.4.3. Relation of Free Volume and Selectivity/Understanding the Behavior of  $\text{O}_2/\text{N}_2$ .** As seen from the Robeson diagram for the  $\text{O}_2/\text{N}_2$  gas pair in Figure 2, the PIM-EA-TB samples in different states are located either close to the upper bound or above it. The separation factor  $\alpha(\text{O}_2/\text{N}_2) = P(\text{O}_2)/P(\text{N}_2)$  (for the given level of  $P(\text{O}_2)$ ) that can be represented as the product  $\alpha(\text{O}_2/\text{N}_2) = \alpha^D \alpha^S$  (as in eq 2). The latter are thus the parameters which are responsible for enhanced selectivity  $\alpha(\text{O}_2/\text{N}_2)$ . It is known<sup>75</sup> that the same trade-off holds for the diagrams of diffusion selectivity  $\alpha^D$  versus diffusivity ( $D_i$ ), as is the case for selectivity and permeability in classical Robeson diagrams.<sup>9</sup> It means that the polymers having higher permeability coefficients (and usually diffusion coefficients) are characterized

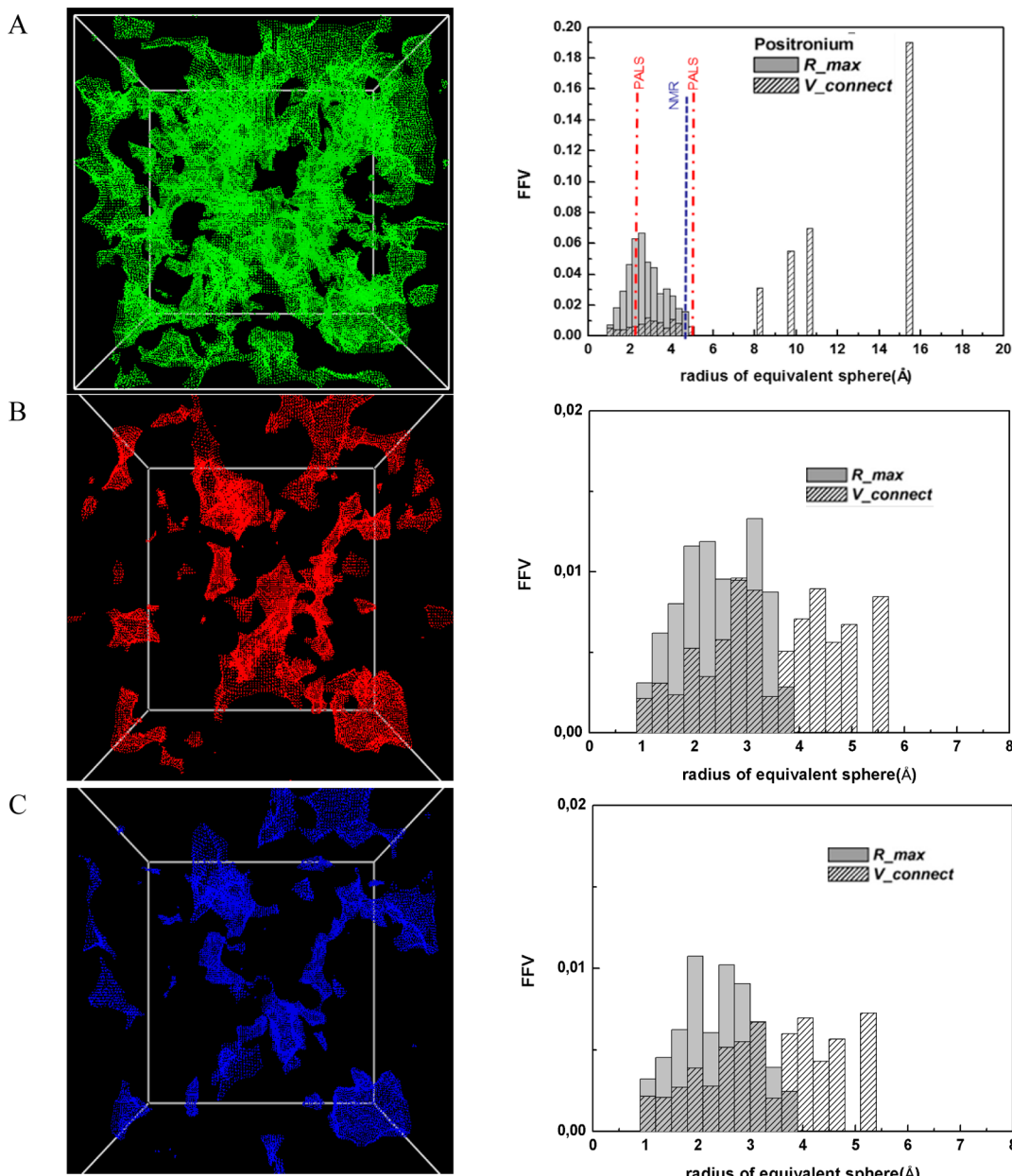


**Figure 8.** 3D model of the free volume distribution in PIM-EA-TB using different probes. Positronium probe (A), oxygen probe (B), and nitrogen probe (C). The graphs on the right show a quantitative evaluation of the averaged size distribution functions using positronium ( $r = 1.1 \text{ \AA}$ ), oxygen ( $r = 1.73 \text{ \AA}$ ) and nitrogen ( $r = 1.82 \text{ \AA}$ ) as probes with the Hofmann–Heuchel method.<sup>47</sup>

**Table 5. Comparison of the Free Volume Element Radius (Å) in PIM-EA-TB Estimated from  $^{129}\text{Xe}$  NMR and MD**

technique	evaluation method	radius (Å)
$^{129}\text{Xe}$ NMR	spherical radius	4.70
	cylindrical radius	3.45
MD	$R_{max}$ approach	2.6
	average radius	2.9
PALS	$R_3$	2.52
	$R_4$	5.07

by lower diffusion selectivity  $\alpha^D$ . On the other hand, solubility selectivity is less sensitive to  $P$  and  $D$  values.<sup>54</sup> Table 2 indicates that  $\alpha^D(\text{O}_2/\text{N}_2)$  is in the range of 2.2–3.5 for different states of PIM-EA-TB. Computer simulations give the values 2.9 (TST) and 3.6 (MD), in good agreement with experimental values.

For different states of PIM-EA-TB,  $\alpha^S(\text{O}_2/\text{N}_2)$  is in the range 1.0–1.8 (average value 1.3), while MD (TST) simulation produced a close value of 1.25. Comparison of these parameters to the  $\alpha^D(\text{O}_2/\text{N}_2)$  and  $\alpha^S(\text{O}_2/\text{N}_2)$  values of a group of relatively permeable polymers with permeability and diffusivity that vary in a wide range (Supporting Information, Table S1) shows that nearly all highly permeable polymers are distinguished by much lower diffusion selectivity as compared to PIM-EA-TB. The only noticeable exception is PIM-1 that has also relatively large  $\alpha^D(\text{O}_2/\text{N}_2)$ , whereas the parameter  $\alpha^S(\text{O}_2/\text{N}_2)$  is more or less the same as in PIM-EA-TB. Comparison of PIM-EA-TB with less permeable polymers shows, for instance, that for polycarbonates<sup>12</sup> the  $\alpha^D(\text{O}_2/\text{N}_2)$  values are in the range 3–5, whereas  $\alpha^S(\text{O}_2/\text{N}_2)$  again are similar to those of PIM-EA-TB. The Database<sup>54</sup> allows making a comparison on a much wider basis. Thus, for numerous polyimides the  $\alpha^D(\text{O}_2/\text{N}_2)$  values

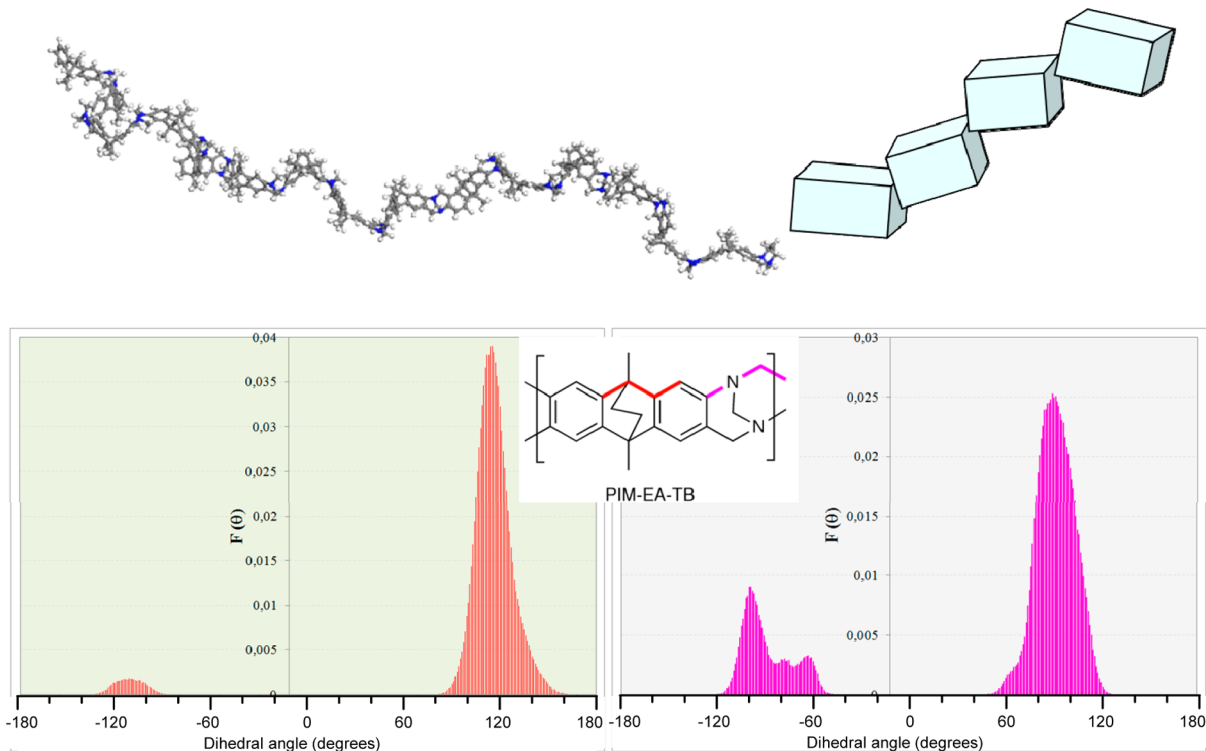


**Figure 9.** PIM-EA-TB polymer structure as a series of rigid rods. The lower section gives the frequency of the dihedral angles of the highlighted bonds.

amount 4–7, for polyvinyl chloride (according to different sources) 2.9–5.9. For this group of less permeable polymers  $\alpha^S(O_2/N_2)$  is in the range 1.1–1.5. It can thus be concluded that the reason for the surprisingly high values  $\alpha(O_2/N_2)$  of PIM-EA-TB (and probably PIM-1) is its unusually large diffusion selectivity. This parameter should depend on connectivity of free volume in the polymer, and the only way to investigate this property is MD simulation.

The modeling studies support the experimental results. The visualization of the accessible free volume regions for different probe molecules, i.e., positronium, oxygen, and nitrogen, is shown in Figure 8A–C. The figures indicate the different amounts of free volume probed in simulation boxes. The oxygen probe can “see” a much larger interconnected free volume than the nitrogen probe and more free volume is accessible for oxygen than for nitrogen. This interconnectivity, a typical characteristic of the polymers of intrinsic microporosity, is responsible for the higher diffusion selectivity  $\alpha^D(O_2/N_2)$ , while the role of solubility selectivity  $\alpha^S(O_2/N_2)$  is negligible. This is confirmed by the quantitative analysis of the size distribution of free volume elements. In the  $R_{max}$  approximation the distributions for  $O_2$  and  $N_2$  are similar, only FFV of oxygen is somewhat greater. On the other hand, the  $V_{connect}$  approximation for oxygen is extended to larger sizes, confirming the greater connectivity for the  $O_2$  probe. These results confirm qualitative considerations made above, based on the gas permeation properties of PIM-EA-TB and other polymers. Analogously, the fundamental difference between PIM-1 and PIM-EA-TB is the presence of intermediate-sized voids according to the  $V_{connect}$  method, and a smaller number of extremely large voids in PIM-EA-TB. This means that gas molecules in PIM-EA-TB have to make more “jumps” from one free volume element to another when diffusing across the membrane, and this is supposed to give the higher size selectivity, while the higher fractional free volume still guarantees a similar permeability as in PIM-1.

**4.4.4. Macromolecular Chain Rigidity, Comparison between MD Simulation and Mechanical Properties.** A common feature of all PIMs is that their exceptional transport and sorption properties can be ascribed to the rigidity of the polymer backbone with highly contorted shape-persistent structure, which creates an unusually high BET surface area. In the previous publication,<sup>10</sup> this rigidity was anticipated via calculation of the energy minima of the dihedral angles of individual groups in the monomeric units. The present work describes a more extensive torsional analysis over the whole backbone, defining with high precision the dihedral angles between three successive chemical bond vectors. The frequency distributions function  $F(\theta)$  of the selected dihedral angles  $\theta$  are calculated and reported for all five chains included in the simulated boxes. There is a maximum for an angle of about 95° of the bicyclic TB units and a minimal contortion in the other plane, while the dihedral angles of the fused rings of the EA unit is almost fixed at a value of 119° with a narrow profile (Figure 9). The very rigid chain of PIM-EA-TB can be represented as series of rigid rods (the bridged bicyclic rings) connected to each other. They are highly inflexible when compared with PIMs that consist of flat ladder parts connected by “joints” (spiro-centers) which represent also the “sites of contortion”.<sup>39,76</sup> A similar dihedral analysis for PIM-1 by Heuchel et al.<sup>39</sup> pointed out that the presence of spiro-centers gives sites of contortion with relative flexibility in the polymer backbone, showing a broad bimodal distribution of dihedral angles associated with the spiro-center. Also according to Chang et al.,<sup>57</sup> the torsional angle results for PIM-1 suggested that the spiro-centers tended to lower the packing efficiency of the chains. The higher frequency of the EA unit compared to the TB dihedral angle reflects the narrower energy pit of the EA unit (Figure 9). The slight shift of the maximum frequency with respect to the minimum in the torsion energy reported by Carta et al.<sup>10</sup> may be partially due to the differences in the calculation algorithm. The smaller second peak appears in the frequency distribution because during the model

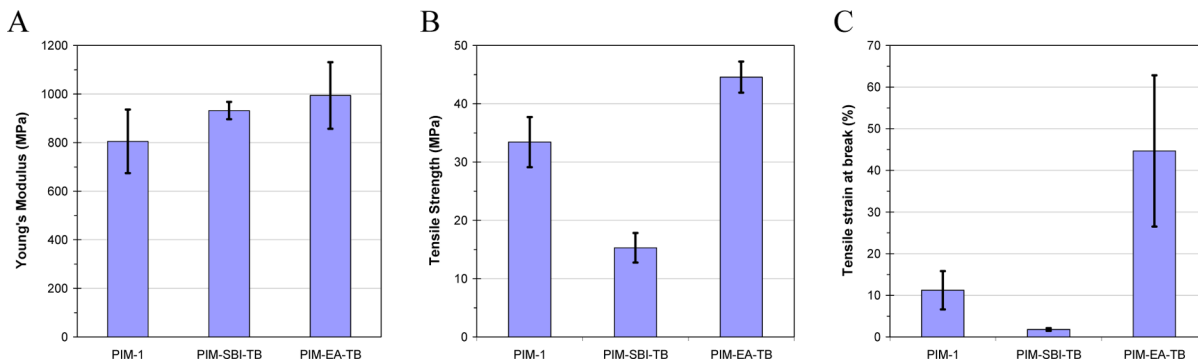


**Figure 10.** Mechanical properties of PIM-EATB in comparison with PIM-1 and PIM-SBI-TB plotted as the average and standard deviation of 4–6 samples. (A) Young's modulus,<sup>10</sup> (B) tensile strength, and (C) maximum elongation.

packing procedure, no matter how long the box construction takes, not all chains can relax to their most favorable conformation, and some chains remain in a frustrated position upon final packing.

As described by Carta et al.,<sup>10</sup> the polymer chain stiffness is reflected in a higher Young's modulus with respect to PIM-1 and PIM-SBI-TB (Figure 10A). Interestingly, whereas PIM-SBI-TB is very brittle, probably due to its relatively low molar mass, the stress–strain curves of PIM-EA-TB showed a noteworthy plastic deformation after the steep initial elastic part of the curve. As a result, also the tensile strength and the maximum elongation are remarkably high for a stiff polymer like PIM-EA-TB (Figure 10B,C). Since measurements were carried out in air, without humidity control, and since PIM-EA-TB shows relatively strong sorption, it cannot be excluded that a few percent of condensables from the air (water vapor, CO<sub>2</sub>) may act as a plasticizer and lubricant, yielding a remarkably tough membrane. Indeed, TGA in general shows a small weight loss at low temperatures, confirming the presence of condensable species.

## 5. CONCLUSIONS

A combination of a vast number of experimental and computational methods highlights in the present study the exceptional transport properties of a novel polymer of intrinsic micro-porosity, PIM-EA-TB, based on ethanoanthracene and Troger's base units in the backbone. For various commercially interesting gas separations, the PIM-EA-TB membranes outperform other PIMs, with data points lying above the 2008 upper bound in the Robeson diagrams for O<sub>2</sub>/N<sub>2</sub>, H<sub>2</sub>/N<sub>2</sub>, H<sub>2</sub>/CO<sub>2</sub>, and H<sub>2</sub>/CH<sub>4</sub>. The lack of efficient packing, in combination with the increased chain rigidity of PIM-EA-TB, forms the main reason for the increased permeability for small gases and the increased size selectivity. In particular, the total lack of flexible sites imparts better molecular sieving characteristics to this polymer compared to PIM-1 and other PIMs, promoting the enhanced diffusivity selectivity for small gases over those with larger kinetic diameters.

The high permeability is typical for PIMs and originates from a very high diffusion coefficient of most gases and from a high solubility coefficient of readily condensable species such as CO<sub>2</sub> in the high fractional free volume. The affinity of PIM-EA-TB for condensable species also results in a relatively high retention of residual casting solvent. Removal of the residual solvent by alcohol treatment leads to an unusually high 5–12 fold increase in the permeability coefficients, mainly by enhancement of the gas diffusion coefficient, *D*, and to a lesser extent by an increase in the solubility, *S*. Relatively strong affinity for CO<sub>2</sub>, related to the presence of the amine groups in the TB moiety, reduces the diffusivity of CO<sub>2</sub> and since this is not fully compensated by

the higher solubility, it results in a relatively low CO<sub>2</sub>/N<sub>2</sub> and CO<sub>2</sub>/CH<sub>4</sub> selectivity.

The two experimental free volume probing methods, PALS and <sup>129</sup>Xe NMR spectroscopy, reveal a relatively large average free volume element size, in the same range of that of PIM-1. PALS furthermore shows a bimodal size distribution, while <sup>129</sup>Xe NMR spectroscopy suggests an exchange between different connected environments. Computer simulated quantification of the FVE size distribution and visualization of the spatial arrangement of the 3-dimensional void structure gives deep insight into the material structure and how these relate to the transport properties. Connectivity of the free volume nanostructure and the available FFV is greater for oxygen than for nitrogen, explaining the relatively high permselectivity,  $\alpha(O_2/N_2)$ , and diffusion selectivity,  $\alpha^D(O_2/N_2)$ , for this gas pair. Molecular dynamics simulations confirmed the trends in the correlation between transport parameters *D* and *S*, with the size and critical properties of the gas molecules.

Only computer modeling could reveal the unique feature of PIM-EA-TB as compared to other PIMs like PIM-1, namely the presence of a number of intermediate-sized voids and fewer extremely large highly interconnected voids. This means that gas molecules in PIM-EA-TB have to make more frequent “jumps” from one free volume element to another when diffusing across the membrane. Combined with the higher chain rigidity of PIM-EA-TB, as revealed by the high energy barriers between the dihedral angles upon analysis of the torsion angles of the polymer chains and by the higher Young's modulus, this gives a direct explanation of the exceptional size selectivity of PIM-EA-TB. This unique study explains both the high permeability of PIM-EA-TB and the high selectivity, via correlation of the transport parameters with its molecular structure and free volume.

Finally, the careful comparison of various methods explains how fundamental differences in the measurement principles and in the boundary conditions for transport, as well as time dependent phenomena and sample conditioning conditions, lead to possible difference in the results. Thus, the overall conclusions are of great value for rationalizing PIM results reported in the literature by different laboratories, using different experimental techniques and measurement procedures.

## ASSOCIATED CONTENT

### Supporting Information

Experimental details, FR-IR results, comparison of the diffusive and the sorptive terms to the permselectivity of glassy polymers, NMR spectra, and free volume element size distribution. This material is available free of charge via the Internet at <http://pubs.acs.org>.

## AUTHOR INFORMATION

### Corresponding Authors

\*(E.T.) E-mail: e.tocci@itm.cnr.it.  
\*(J.C.J.) E-mail: jc.jansen@itm.cnr.it.

### Notes

The authors declare no competing financial interest.

## ACKNOWLEDGMENTS

Part of the work leading to these results has received funding from the European Community's Seventh Framework Programme (FP7/2007-2013) under Grant Agreement No. NMP3-SL-2009-228631, Project DoubleNanoMem, and the OKhNM (RAS) program.

## REFERENCES

- (1) McKeown, N. B. *ISRN Mater. Sci.* **2012**, No. 513986.
- (2) McKeown, N. B.; Budd, P. M. *Macromolecules* **2010**, *43*, 5163–5176.
- (3) Budd, P. M.; Ghanem, B. S.; Makhseed, S.; McKeown, N. B.; Msayib, K. J.; Tattershall, C. E. *Chem. Commun.* **2004**, 230–231.
- (4) Budd, P. M.; Elabas, E. S.; Ghanem, B. S.; Makhseed, S.; McKeown, N. B.; Msayib, K. J.; Tattershall, C. E.; Wang, D. *Adv. Mater.* **2004**, *16*, 456–459.
- (5) Budd, P. M.; McKeown, N. B.; Ghanem, B. S.; Msayib, K. J.; Fritsch, D.; Starannikova, L.; Belov, N.; Sanfirrova, O.; Yampolskii, Y. P.; Shantarovich, V. *J. Membr. Sci.* **2008**, *325*, 851–860.
- (6) Budd, P. M.; Msayib, K. J.; Tattershall, C. E.; Ghanem, B. S.; Reynolds, K. J.; McKeown, N. B.; Fritsch, D. *J. Membr. Sci.* **2005**, *251*, 263–269.
- (7) Thomas, S.; Pinna, I.; Du, N. Y.; Guiver, M. D. *J. Membr. Sci.* **2009**, *333*, 125–131.
- (8) Staiger, C. L.; Pas, S. J.; Hill, A. J.; Cornelius, C. *J. Chem. Mater.* **2008**, *20*, 2606–2608.
- (9) Robeson, L. M. *J. Membr. Sci.* **2008**, *320*, 390–400.
- (10) Carta, M.; Malpass-Evans, R.; Croad, M.; Rogan, Y.; Jansen, J. C.; Bernardo, P.; Bazzarelli, F.; McKeown, N. B. *Science* **2013**, *339*, 303–307.
- (11) Carta, M.; Croad, M.; Malpass-Evans, R.; Jansen, J. C.; Bernardo, P.; Clarizia, G.; Friess, K.; Lanč, M.; McKeown, N. B. *Adv. Mater.* **2014**, *26*–*21*, 3526–3531.
- (12) Pixton, M. R.; Paul, D. R. In *Polymeric Gas Separation Membranes*, Eds. Paul, D. R., Yampolskii, Yu. P., CRC Press: Boca Raton, FL, 1994; p83.
- (13) Robeson, L. M. *J. Membr. Sci.* **1991**, *62*, 165–185.
- (14) Alentiev, A. Doctor of Science Thesis, Topchiev Institute of Petrochemical Synthesis: Moscow, 2003.
- (15) Masuda, T.; Iguchi, Y.; Tang, B.-Z.; Higashimura, T. *Polymer* **1988**, *29*, 2041–2049.
- (16) Merkel, T. C.; Bondar, V.; Nagai, K.; Freeman, B. D. *J. Polym. Sci., Part B: Polym. Phys.* **2000**, *38*, 273–296.
- (17) Nagai, K.; Masuda, T.; Nakagawa, T.; Freeman, B. D.; Pinna, I. *Prog. Polym. Sci.* **2001**, *26*, 721–798.
- (18) Hill, A. J.; Pas, S. J.; Bastow, T. J.; Burgar, M. I.; Nagai, K.; Toy, L. G.; Freeman, B. D. *J. Membr. Sci.* **2004**, *243*, 37–44.
- (19) Yampolskii, Yu.; Alentiev, A.; Bondarenko, G.; Kostina, Y.; Heuchel, M. *Ind. Eng. Chem. Res.* **2010**, *49*, 12031–12037.
- (20) Terskikh, V. V.; Moudrakovski, I. L.; Breeze, S. R.; Lang, S.; Ratcliffe, C. I.; Ripmeester, J. A.; Sayari, A. *Langmuir* **2002**, *18*, 5653–5656.
- (21) Simonutti, R.; Bracco, S.; Comotti, A.; Mauri, M.; Sozzani, P. *Chem. Mater.* **2006**, *18*, 4651–4657.
- (22) Comotti, A.; Bracco, S.; Ferretti, L.; Mauri, M.; Simonutti, R.; Sozzani, P. *Chem. Commun.* **2007**, 350–352.
- (23) Bracco, S.; Valsesia, P.; Ferretti, L.; Sozzani, P.; Mauri, M.; Comotti, A. *Microporous Mesoporous Mater.* **2008**, *107*, 102–107.
- (24) Crank, J. *The mathematics of diffusion*, 2nd ed.; Clarendon Press: Oxford, U.K., 1975.
- (25) Mason, C. R.; Maynard-Atem, L.; Al-Harbi, N. M.; Budd, P. M.; Bernardo, P.; Bazzarelli, F.; Clarizia, G.; Jansen, J. C. *Macromolecules* **2011**, *44*, 6471–6479.
- (26) Bushell, A. F.; Attfield, M. P.; Mason, C. R.; Budd, P. M.; Yampolskii, Yu.P.; Starannikova, L.; Rebrov, A.; Bazzarelli, F.; Bernardo, P.; Jansen, J. C.; Lanč, M.; Friess, K.; Shantarovich, V.; Gustov, V.; Isaeva, V. *J. Membr. Sci.* **2013**, *42*, 48–62.
- (27) Friess, K.; Hynek, V.; Šípek, M.; Kujawski, W. M.; Vopicka, O.; Zgažar, M.; Kujawski, M. W. *Sep. Purif. Technol.* **2011**, *80* (3), 418–427.
- (28) Friess, K.; Jansen, J. C.; Vopicka, O.; Randová, A.; Hynek, V.; Šípek, M.; Bartovská, L.; Izák, P.; Dingemans, M.; Dewulf, J.; Van Langenhove, H.; Drioli, E. *J. Membr. Sci.* **2009**, *338* (1–2), 161–174.
- (29) Vieth, W. R.; Sladek, K. *J. Colloid Sci.* **1965**, *20*, 1014–1033.
- (30) Yampolskii, Y.; Shantarovich, V. Positron annihilation lifetime spectroscopy and other methods for free volume evaluation in polymers. In *Materials Science of Membranes for Gas and Vapor Separation*; Yampolskii, Yu., Pinna, I., Freeman, B. D., Eds.; John Wiley & Sons: Chichester, England, 2006; Chapter 6, pp 191–210.
- (31) Belousova, E.; Gustov, V.; Medintseva, T.; Polyakova, A.; Prut, E.; Shantarovich, V. Progress in Positron Annihilation. *Mater. Sci. Forum* **2011**, *666*, 81.
- (32) Tao, J. *J. Chem. Phys.* **1972**, *56*, 5499–5510.
- (33) Eldrup, M.; Lightbody, D.; Sherwood, J. N. *Chem. Phys.* **1981**, *63*, 51–58.
- (34) Shantarovich, V.; Gustov, V.; Polyakova, A.; Belousova, E.; Filimonov, M.; Yampolskii, Yu. *Phys. Stat. Sol. C6* **2009**, *11*, 2387.
- (35) van Miltenburg, A.; de Ménorval, L. C.; Stöcker, M. *Catal. Today* **2011**, *168*, 57–62.
- (36) Demarquay, J.; Fraissard, J. *Chem. Phys. Lett.* **1987**, *136*, 314–318.
- (37) *Material Studio (6.0) package of Accelrys. Polymer User Guide. Polymerizer section*; Accelrys Software Inc.: San Diego, CA, 2009.
- (38) Sun, H.; Rigby, D. *Spectrochim. Acta* **1997**, *53A*, 1301–1323.
- (39) Heuchel, M.; Fritsch, D.; Budd, P. M.; McKeown, N. B.; Hofmann, D. *J. Membr. Sci.* **2008**, *318*, 84–99.
- (40) Theodorou, D. N.; Suter, U. W. *Macromolecules* **1985**, *18*, 1467–1478.
- (41) Theodorou, D. N.; Suter, U. W. *Macromolecules* **1986**, *19*, 139–154.
- (42) Gusev, A. A.; Arizzi, S.; Suter, U. W. *J. Chem. Phys.* **1993**, *99*, 2221–2227.
- (43) Gusev, A. A.; Suter, U. W. *J. Chem. Phys.* **1993**, *99*, 2228–2234.
- (44) *Gsnet & Gsdif Macros*; Accelrys Inc.: San Diego, CA, 1999.
- (45) Haile, J. M. *Molecular Dynamics Simulation*; Wiley: New York, 1992.
- (46) Metropolis, N.; Rosenbluth, A. W.; Rosenbluth, M. N.; Teller, A. H.; Teller, E. *J. Chem. Phys.* **1953**, *21*, 1087–1092.
- (47) Hofmann, D.; Heuchel, M.; Yampolskii, Y.; Khotimskii, V.; Shantarovich, V. *Macromolecules* **2002**, *35*, 2129–2140.
- (48) van Krevelen, D. W.; te Nijenhuis, K. *Properties of Polymers*, 4th ed.; Elsevier: Amsterdam, 2009.
- (49) Macchione, M.; Jansen, J. C.; Deluca, G.; Tocci, E.; Longer, M.; Drioli, E.; De Luca, G. *Polymer* **2007**, *48*, 2619–2635.
- (50) Chen, R. H.; Hwa, H.-D. *Carbohydr. Polym.* **1996**, *29*, 353–358.
- (51) Toi, K.; Paul, D. R. *Macromolecules* **1982**, *15*, 1104–1107.
- (52) Budd, P. M. et al. Unpublished results.
- (53) Zhou, J.; Zhu, X.; Hu, J.; Liu, H.; Hu, Y.; Jiang, J. *Phys. Chem. Chem. Phys.* **2014**, *16*, 6075–6083.
- (54) Database “Gas permeation parameters of glassy polymers”, No. 3585; Informregistr RF: Moscow, 1998.
- (55) Teplyakov, V.; Meares, P. *Gas Sep. Purif.* **1990**, *4*, 66–73.
- (56) Mason, C. R.; Maynard-Atem, L.; Heard, K. W. J.; Satilmis, B.; Budd, P. M.; Friess, K.; Lanč, M.; Bernardo, P.; Clarizia, G.; Jansen, J. C. *Macromolecules* **2014**, *47* (3), 1021–1029.
- (57) Chang, K.-S.; Tung, K.-L.; Lin, Y.-F.; Lin, H.-Y. *RSC Adv.* **2013**, *3*, 10403–10413.
- (58) Yampolskii, Y. *Macromolecules* **2012**, *45*, 3298–3311.
- (59) Heuchel, M.; Hofmann, D.; Pullumbi, P. *Macromolecules* **2004**, *37*, 201.

- (60) Neyertz, S.; Brown, D.; Pandiyan, S.; van der Vegt, N. F. A. *Macromolecules* **2010**, *43*, 7813–7827.
- (61) Li, P.; Chung, T. S.; Paul, D. R. *J. Membr. Sci.* **2014**, *450*, 380–388.
- (62) Robeson, L. M.; Smith, Z. P.; Freeman, B. D.; Paul, D. R. *J. Membr. Sci.* **2014**, *453*, 71–83.
- (63) Unpublished results from the European Community's Seventh Framework Programme (FP7/2007–2013), grant agreement no. NMP3-SL-2009-228631, project DoubleNanoMem.
- (64) Vopička, O.; Friess, K.; Hynek, V.; Sysel, P.; Zgažar, M.; Šípek, M.; Pilnáček, K.; Lanč, M.; Jansen, J. C.; Mason, C. R.; Budd, P. M. *J. Memb. Sci.* **2013**, *434*, 148–160.
- (65) Goldanskii, V. I.; Mokrushin, A. D.; Tatur, A. O.; Shantarovich, V. P. *Appl. Phys.* **1975**, *5*, 379–382.
- (66) Gringolts, M.; Bermeshev, M.; Yampolskii, Yu.; Starannikova, L.; Shantarovich, V.; Finkelstein, E. *Macromolecules* **2010**, *43*, 7165–7172.
- (67) Lima de Miranda, R.; Krause, J.; Raetzke, K.; Faupel, F.; Fritsch, D.; Abetz, V.; Budd, P. M.; Selbie, J. D.; McKeown, N. B.; Ghanem, B. S. *Phys. Status Solidi (RRL)* **2007**, *1*, 190–192.
- (68) Emmler, T.; Heinrich, K.; Fritsch, D.; Budd, P. M.; Chaukura, N.; Ehlers, D.; Raetzke, K.; Faupel, F. *Macromolecules* **2010**, *43*, 6075–6084.
- (69) Mauri, M.; Simonutti, R. *Materials* **2012**, *5*, 1722–1739.
- (70) Matteucci, S.; Yampolskii, Y.; Freeman, B. D.; Pinnau, I. Transport of Gases and Vapors in Glassy and Rubbery Polymers. In *Materials Science of Membranes for Gas and Vapor Separation*; Yampolskii, Yu., Pinnau, I., Freeman, B. D., Eds.; John Wiley & Sons: Chichester, England, 2006; Chapter 1, pp 1–47.
- (71) Rogan, Y.; Malpass-Evans, R.; Carta, M.; Lee, M.; Jansen, J. C.; Bernardo, P.; Clarizia, G.; Tocci, E.; Friess, K.; Lanč, M.; McKeown, N. B. *J. Mater. Chem. A* **2014**, *2/14*, 4874–4877.
- (72) Jansen, J. C.; Macchione, M.; Tocci, E.; De Lorenzo, L.; Yampolskii, Y. P.; Sanfirova, O.; Shantarovich, V. P.; Hofmann, D.; Drioli, E. *Macromolecules* **2009**, *42*, 7589–7604.
- (73) Hofmann, D.; Entrialgo-Castano, M.; Lerbet, A.; Heuchel, M.; Yampolskii, Y. *Macromolecules* **2003**, *36*, 8528–8538.
- (74) Hofmann, D.; Heuchel, M.; Yampolskii, Y.; Khotimskii, V.; Shantarovich, V. *Macromolecules* **2002**, *35*, 2129–2140.
- (75) Alentiev, A.; Yampolskii, Yu. *Ind. Eng. Chem. Res.* **2013**, *52*, 8864–8874.
- (76) Guiver, M. D.; Lee, Y. M. *Science* **2013**, *339*, 284–285.